Long-lived Deep Coherent Vortices in the Northeast Atlantic Ocean

Ashwita Chouksey[1], Jonathan Gula[1,2] and Xavier Carton[1]

[1]Univ Brest, CNRS, IRD, Ifremer, Laboratoire d'Océanographie Physique et Spatiale (LOPS), IUEM, 29280, Brest, France
[2]Institut Universitaire de France (IUF), France

Key Points:

- Deep anticyclones are larger, more energetic, and longer-lived than deep cyclones
- Strong anticyclonic meddies often destroy their cyclonic companions
- Meddies interact with anticyclonic vortices formed of Antarctic Intermediate Water near the Moroccan coast
- Multiple interactions occur between meddies, Canary anticyclones, and deep cyclones generated near the West African coast

Corresponding author: Ashwita Chouksey, ashwita.chouksey@univ-brest.fr

Abstract

Ocean eddies play an important role in the distribution of heat, salt, and other tracers in the global ocean. But while surface eddies have been studied extensively, deeper eddies are less well understood. Here we study deep coherent vortices (DCVs) in the Northeast Atlantic Ocean using a high resolution numerical simulation. We perform a census of the DCVs on the 27.60 kg/m^3 isopycnal, at the depth of $700 - 1500$ m, where DCVs of Mediterranean water (meddies) propagate. We detect a large number of DCVs, with maxima around continental shelves, and islands, dominated by small and short-lived cyclones. However, the large and long-lived DCVs are mostly anticyclonic. Among the long-lived DCVs, anticyclonic meddies, stand out. They grow in size by merging with other anticyclonic meddies. Cyclonic meddies are also regularly formed, but most of them are destroyed near their formation sites due to the presence of the energetic anticyclonic meddies, which destroy cyclones by straining and wrapping the positive vorticity around their core. During their life cycle, as they propagate to the southwest, anticyclonic meddies can interact with other DCVs, including anticyclones containing Antarctic Intermediate Water generated near the Moroccan coast, Canary anticyclonic DCVs and cyclonic DCVs generated south of 30°N along the African continental shelf. With these latter, they can form dipoles, and with the former, they co-rotate pro tempore. Thus, a more detailed view of the life cycle of anticyclonic meddies is proposed: they grow by merging, undergo multiple interactions along their path, and they decay at low latitudes.

Plain Language Summary

The study focuses on eddies in the Northeast Atlantic Ocean at depths between 700 and 1500 m. Using a high-resolution numerical ocean model and an eddy detection method, we identify deep eddies and quantify their physical characteristics (radius, lifetime, number of cyclones versus anticyclones). Cyclones are more frequent among short-lived eddies travelling over short distances, whereas anticyclones are more frequent among long-lived eddies travelling over long distances. The anticyclones containing Mediterranean Water first remain near their generation site, grow by fusion and destroy their cyclonic counterparts by elongation. Then, they move away from their generation sites and interact with other deep anticyclonic and cyclonic eddies. This study sheds new light on the richness of deep eddy dynamics in the ocean.

1 Introduction

Oceanic eddies have been extensively studied in the Northeast Atlantic (NEA) Ocean (e.g., Arhan et al., 1994; Johnson & Stevens, 2000; Schütte et al., 2016). Most studies have been devoted to the mesoscale eddies with a surface signature, such as those found near the Azores Islands (Carracedo et al., 2014), the Canary Basin (Mason et al., 2011), the Cape Verde Archipelago (Peña-Izquierdo et al., 2012), and the Gulf of Guinea (Ingham, 1970). However, fewer studies have explored deep vortices in the NEA, with the exception of those describing eddies formed of Mediterranean Water (MW), usually called "meddies" (McDowell & Rossby, 1978), and more rarely, some describing eddies detected along the African coast and in particular near the Canary Current system McCoy et al. (2020).

Deep coherent vortices (DCVs) refer to the eddies found below the mixed layer depth and with a dominant horizontal motion and a closed fluid circulation in their core due to the Coriolis force and to the buoyancy effects (McWilliams, 1985). The fluid circulation may be anticyclonic or cyclonic. An anticyclonic DCV is associated with isopycnals forming a convex lens shape in the vertical around a weakly stratified core. A cyclonic DCV is associated with a narrowing of the isopycnals in the vertical.

To the best of our knowledge, no type of DCV other than meddies have been extensively studied in the NEA, and the few observations available concern only anticyclonic DCVs. Here we focus on long-lived DCVs in the NEA on the isopycnal $\sigma = 27.60$ kg/m^3, on which meddies are present. We investigate their dynamics in detail, including the formation and life cycle of DCVs, and their interactions with other DCVs, using a high-resolution model.

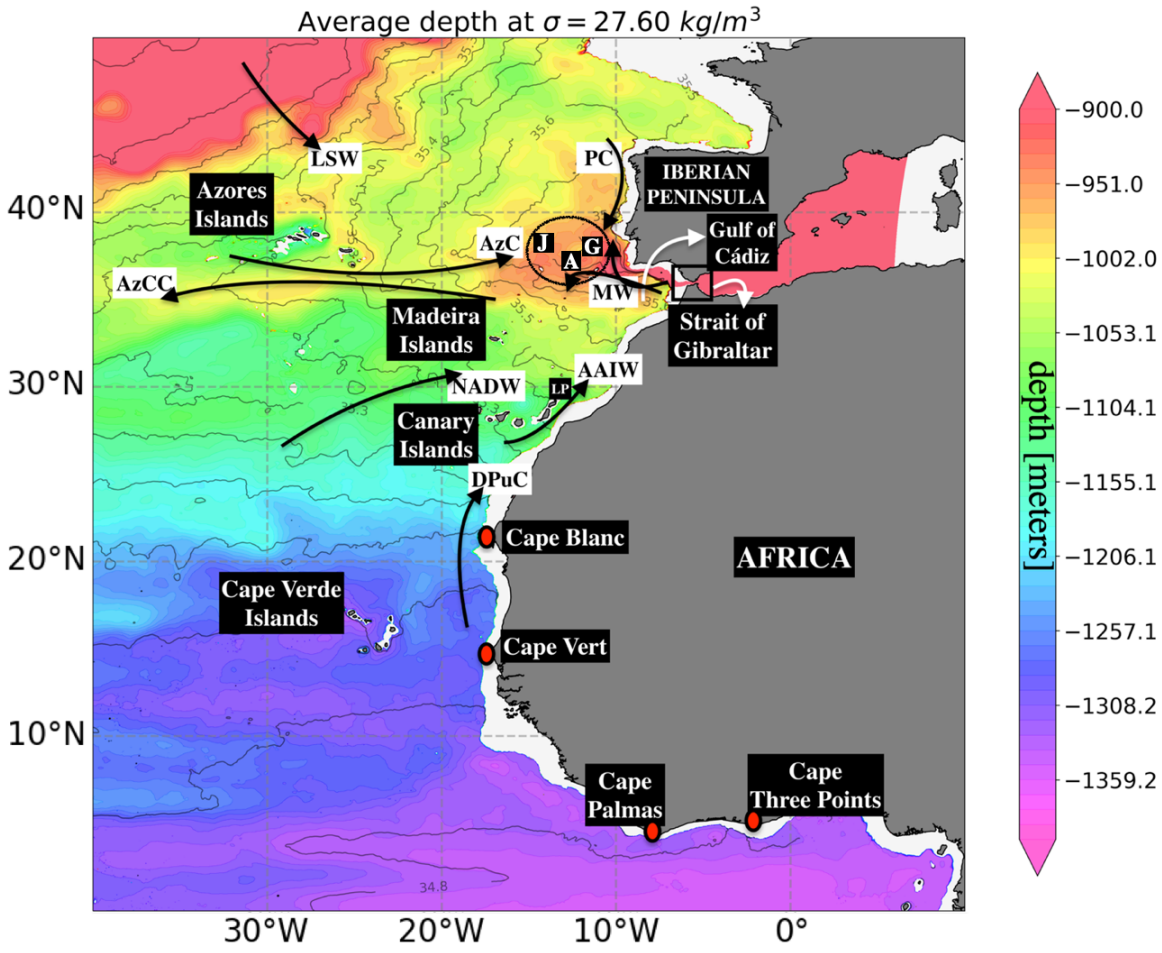

Figure 1. Map of the Northeast Atlantic Ocean ($0° - 50°$N, $40°$W $-10°$E) shows the major regional currents and water masses along the isopycnal, $\sigma = 27.60$ kg/m^3. The currents and water masses are indicated by black text and thick black arrows; they include PC (Portugal Current), AzC (Azores Current), AzCC (Azores Countercurrent), DPuC (Deep Poleward Undercurrent), MW (Mediterranean Water), LSW (Labrador Sea Water), NADW (North Atlantic Deep Water), and AAIW (Antarctic Intermediate Water). The black circled region denotes the Horseshoe Seamounts indicating Gorringe bank (G), Ampère (A), and Josephine (J). The red dots represent the different capes. The color shading shows the average depth in meters with superimposed average salinity contours in g/kg.

The main regional currents in the NEA found along the isopycnal $\sigma = 27.60$ kg/m^3 (referenced to the surface) are represented in the schematic shown in Figure 1. The average depth for this isopycnal in the NEA is between $700 - 1500$ m, being shallower north of $30°$N than south of $30°$N. This region contains several important water masses such as MW, Antarctic Intermediate Water (AAIW), Labrador Sea Water (LSW), and North Atlantic

Deep Water (NADW). Depending on where they are formed, DCVs contain one of these types of water masses and, due to their strong coherence, tend to retain much of it in their core during their lifetime.

Meddies, containing MW, are salty and warm DCVs intensified on the $\sigma = 27.60$ kg/m^3 isopycnal (McDowell & Rossby, 1978), approximately at 1000 m depth. Meddies form due to instabilities of the MW outflow, which enters the NEA via the Strait of Gibraltar (Figure 1), and veers north along the continental slope after exiting the strait at about $800 - 1200$ m depth (Ambar et al., 2002). Many generation mechanisms have been proposed for meddies, including baroclinic instability (Chérubin et al., 2007; Duarte et al., 2011); convective mixing followed by geostrophic adjustment, turbulent mixing and entrainment (McWilliams, 1985; Käse et al., 1989); friction of the MW outflow against the continental slopes, boundary currents or seamounts (D'Asaro, 1988a, 1988b); and coastal or topographic effects (Pichevin & Nof, 1996; Chérubin et al., 2000).

Despite the fact that historical observations show a preference for anticyclones, meddies can be both cyclonic ($C_{meddies}$) and anticyclonic ($A_{meddies}$). $C_{meddies}$ have been observed along with $A_{meddies}$, for example by Richardson et al. (2000) and X. Carton et al. (2002). A large population of $C_{meddies}$ exists near the Gulf of Cádiz. $C_{meddies}$ have a concave shape, in contrast with the convex shape of $A_{meddies}$. The vertical extent of $C_{meddies}$ is $600 - 1300$ m and azimuthal velocity of $0.1 - 0.16$ m/s, while $A_{meddies}$ can extend $500 - 1500$ m (X. Carton et al., 2002) with maximum azimuthal velocities of $0.1 - 0.3$ m/s (Armi et al., 1989). $A_{meddies}$ with radii of $10 - 15$ km have been found near the subtropics ($35° - 45°$N) and with larger radii of $25 - 30$ km further south ($25° - 35°$N) in the northern tropics (Bashmachnikov & Carton, 2012). $C_{meddies}$ have lower salinity ($36.2 - 36.4$ psu) and temperature ($11° - 12°$C) (Ambar et al., 2008) compared to the $A_{meddies}$ with corresponding salinity (temperature) of $36.2 - 36.6$ psu ($11.4° - 13°$C) (X. Carton et al., 2002). $C_{meddies}$ and $A_{meddies}$ are expected to drift northwestward and southwestward, respectively, under the influence of the $\beta-$effect (Pichevin & Nof, 1996). Other mechanisms, such as advection and diffusion processes by barotropic or baroclinic currents (Beckmann & Käse, 1989), or interaction with topographic slopes (Richardson et al., 2000) also account for their overall drift.

Another major current system that affects the local circulation and generates DCVs is the Canary Current (CC). The CC flows in the Canary Basin ($10° - 40°$N) and extends to depths of $700 - 1400$ m (Casanova-Masjoan et al., 2020). Its poleward extension through the Lanzarote Passage (LP) can reach depths of 1300 m and transports NACW ($0 - 600$ m), AAIW ($600 - 1100$ m), and MW (900 m - seafloor) (Machín & Pelegrí, 2009). The interaction of the salty MW and the fresher AAIW has been discussed in many studies (cf. McDowell & Rossby, 1978). The deeper northward flow below the coastal jet of the CC transports the AAIW with 80% dilution ($6° - 7.9°$C and $34.9 - 35$ psu, cf. Carracedo et al., 2012) along the passage between the Canary Islands and the African coast (LP, Figure 1) and drifts further to the north in the Gulf of Cádiz, in the isopycnal range $\sigma = 27.2 - 27.65$ kg/m^3 (cf. Louarn & Morin, 2011). The interaction of the current with the Canary Islands leads to the generation of DCVs, which then move offshore, south of the CC (Pelegrí et al., 2005). This region has been identified as a hot-spot for the generation of anticyclonic DCVs containing anomalously cold and fresh water McCoy et al. (2020).

Previous studies have focused mostly on $A_{meddies}$, which take the form of long-lived anticyclonic DCVs in the NEA, north of 30°N. South of 30°N, most of the coherent vortices have been identified at the surface or near the mixed layer. However, the presence of several deep-reaching currents interacting with continental slopes and islands in the NEA should generate a variety of DCVs. Aguiar et al. (2013) question why short-lived meddies disappear and further hypothesize that the fate of long-lived meddies is related to eddy merging. They also document that small $C_{meddies}$ disappear faster near the coastal boundary and that only a few can survive more than 90 days, likely because their core lies deeper than

the short-lived $C_{meddies}$. But the fate of the long-lived $C_{meddies}$ remains an open question.

The aim of the present study is to provide a comprehensive census of DCVs in the NEA along the $\sigma = 27.60$ kg/m^3 isopycnal, using a high-resolution numerical model with a horizontal resolution of $\Delta x = 3$ km able to reproduce DCVs with radii > 15 km, and an eddy identification algorithm. We compute the spatial distribution, physical properties (polarity, radius, and velocity), and propagation in space and time for the DCVs, to address the questions raised by Aguiar et al. (2013) regarding the fate of long-lived and short-lived meddies. We also investigate the life cycle of long-lived $A_{meddies}$, with special emphasis on their growth and decay, as well as their interactions with long-lived DCVs of different origin and containing different water masses, including: anticyclones containing AAIW, anticyclones containing Canary Water, and cyclones containing water masses from south of 30°N.

This paper is organised as follows: Section 2 presents the numerical model and the *py-eddy-tracker* algorithm used for eddy identification and tracking. The results presented in Section 3 are divided into statistics for all eddies (Section 3.1), and the study of the life cycle of meddies and their interaction with the DCVs of different origin (Section 3.2). The conclusions are presented in Section 4.

2 Materials and Methods

2.1 Numerical ocean model

In this study, we use the Coastal and Regional Ocean Community (CROCO) model. The CROCO model is based on the Regional Ocean Model System (ROMS) primitive equation (Shchepetkin & McWilliams, 2005) and solves the free surface, hydrostatic, and primitive equations on an Arakawa-C grid with terrain-following curvilinear coordinates. Our numerical simulation, called GIGATL3, covers the entire Atlantic Ocean and consists of 3002×4002 grid points with a horizontal resolution of $\Delta x = 3$ km and 100 vertical sigma levels (distributed unevenly). To supply boundary and initial conditions, we used the Simple Ocean Data Assimilation (SODA, J. A. Carton & Giese, 2008). The simulation was forced by hourly atmospheric forcing from the Climate Forecast System Reanalysis (CFSR, Saha et al., 2010) and bathymetry was taken from the SRTM30_PLUS dataset (Becker et al., 2009). The $k-\epsilon$ turbulence closure scheme was employed to parameterize vertical mixing (Umlauf & Burchard, 2003), with the Canuto A stability function formulation applied (Canuto et al., 2001). We accounted for bottom friction using a logarithmic law of the wall with a roughness length of $Z_0 = 0.01$ m. For more information on the CROCO model and its source code, see Gula et al. (2021).

The model ran for 9.5 years, excluding the first 2.5 years as spin-up. We analyzed the remaining 7 years, with 12 hours output, from July 2006 to July 2013 over the NEA, $0° - 50°$N, $40°$W $-10°$E.

2.2 Phenomenology

To verify that the model can generate realistic meddies, we compared our model's output to an observational section taken along 8.5°W showing both an A_{meddy} and a C_{meddy} (Figure 2a). The observational data were obtained during the SEMANE (Suivi des Eaux Méditerranéennes en Atlantique Nord-Est) 1999 experiment in the Gulf of Cádiz by the French Hydrographic and Oceanographic Service. Two example model sections taken along 9.1°W, one including an A_{meddy} and one including a C_{meddy}, are shown in Figure 2b,c, for comparison. They demonstrate a qualitative agreement in the structure of the meddies.

In the observations (Figure 2a), the A_{meddy} lies between $34° - 35°$N with a radius of 50 km, a thickness of 900 m, and a core salinity of 36.39 g/kg; and the C_{meddy} lies between

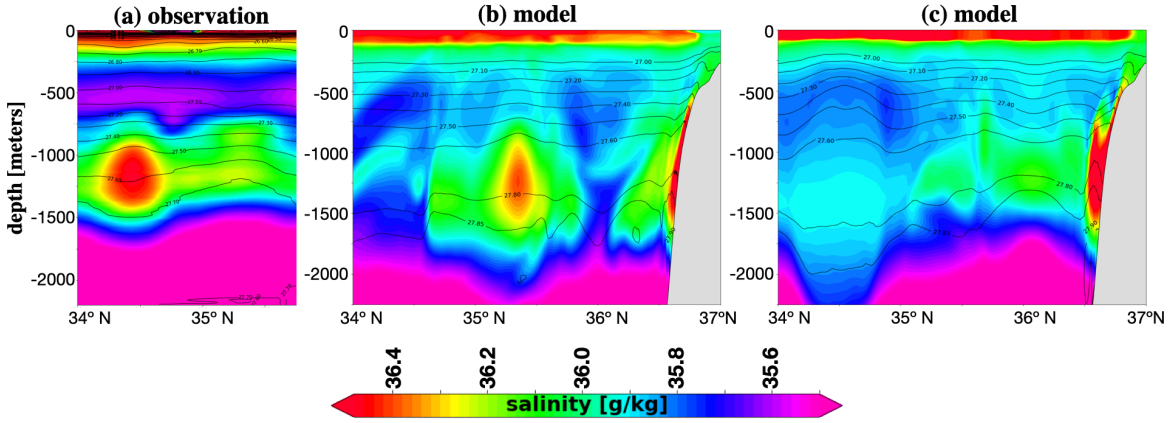

Figure 2. Vertical sections of salinity from (a) the SEMANE experiment along 8.5°W, showing an anticyclonic meddy (A_{meddy}, 34° − 35°N) and a cyclonic meddy (C_{meddy}, 34.5° − 35.8°N), (b) model output along 9.1°W, showing an A_{meddy} (28 March 2008, 34.5° − 35.8°N); and (c) model output along 9.1°W, showing a C_{meddy} (04 December 2008, 35.6° − 36.5°N), and an anticyclone containing Antarctic Intermediate Water (A_{aaiw}, 34° − 35°N). The color shading indicates the salinity (in g/kg) with overlaid black contours of isopycnals (in kg/m^3).

35° − 36°N with a radius of 50 km, a thickness of 800 m, and a core salinity of 36.17 g/kg. The modeled A_{meddy} is shown in Figure 2b, with a core located between 34.5° − 35.8°N, a salinity core of 36.3 g/kg about 1000 m thick, similar to the observed section (Figure 2a). The difference between the observed (Figure 2a) and the modeled A_{meddy} (Figure 2b) is that the observed one has a fully-developed eddy core, while the modelled one has been generated more recently. The modeled C_{meddy} (35.6° − 36.5°N) in Figure 2c is also in the 800 − 1600 m depth range and its salinity (36.06 g/kg) is close to the observed one in Figure 2a (36.17 g/kg).

The Mediterranean outflow is clearly visible near the continental shelf (36.5°N) with a salinity of 36.5 g/kg (Figure 2b, c), similar to the SEMANE 1999 section (not shown here, but equal to 36.6 g/kg). The homogeneous core to the left of the C_{meddy}, between 34° − 35°N (Figure 2c), contains a bi-convex anticyclonic vortex lens containing AAIW (A_{aaiw}). The presence of AAIW near the Moroccan shelf is documented by Louarn and Morin (2011) and Carracedo et al. (2016). These studies note a salinity of 35.6 g/kg for the AAIW, which is also seen in our model output for the vortex core (Figure 2c).

2.3 Eddy Identification Algorithm

To detect the DCVs, we adapt the *py-eddy-tracker*, eddy tracking algorithm of Mason et al. (2014). The DCVs here are identified using the Okubo-Weiss parameter (OW, Okubo (1970); Weiss (1991)) and the geometric criteria defined in Mason et al. (2014). The OW parameter assigns negative values to regions dominated by vorticity and positive values to regions dominated by strain and is defined as:

$$OW = s_n^2 + s_s^2 - \omega^2 \tag{1}$$

where s_n is the normal strain ($\frac{\partial u}{\partial x} - \frac{\partial v}{\partial y}$), s_s is the shear strain ($\frac{\partial v}{\partial x} + \frac{\partial u}{\partial y}$), and ω is the relative vorticity ($\frac{\partial v}{\partial x} - \frac{\partial u}{\partial y}$); with u and v the horizontal velocity components. The presence of an eddy is indicated by negative values of OW. Here we select closed contours of OW with values from -10^{-12} s^{-2} to -10^{-9} s^{-2} with an increment of -10^{-12} to detect eddies and to define

the contour of the eddy. The upper bound of OW (-10^{-12} s^{-2}) falls among the threshold values suggested by Chelton et al. (2007) for eddy detection, and the lower bound -10^{-9} s^{-2} catches the core of the strongest eddies. Each contour is tested sequentially, starting from the largest one, and must meet two criteria related to its shape to be considered as an eddy:

- The shape error, which quantifies the deformation of the eddy, has to be less than 55% (Kurian et al., 2011; Mason et al., 2014)
- The number of pixels (P) inside the contour must satisfy $10 \leq P \leq 2000$

2.4 Eddy Tracking algorithm

Detection is performed every 12 hours for ~ 7 years from 03 July 2006 – 30 July 2013. We use the tracking method described in Pegliasco et al. (2022) to link contours detected at different time steps to form tracks. The procedure is based on the overlap between contours, which must be $\geq 20\%$ between two consecutive time steps. Only tracks longer than 21 days are considered in order to filter out short-lived vortices. A virtual time step of one day is used to allow the track to continue if only one detection is missing. The choice of the virtual time step has no significant effect on the results presented here (tested with different values, from one day to five days).

2.5 Assessment of the algorithm

We present here an example of detection performed along the isopycnal surface 27.60 kg/m^3, which lies in the average depth range of 700 – 1500 m in the NEA domain (Figure 1). Maps of the relative vorticity and the OW parameter are shown with contours superimposed

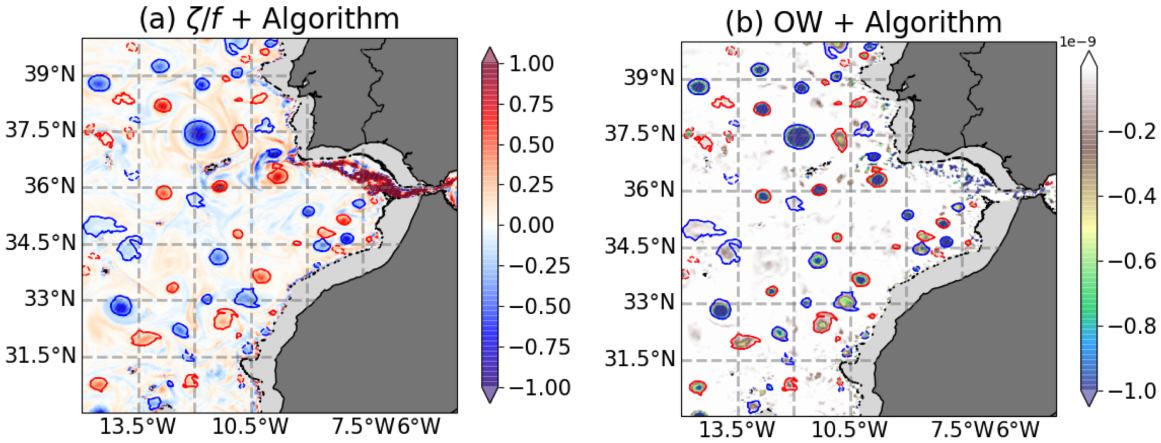

Figure 3. (a) Relative vorticity (ζ/f) and (b) OW parameter (in s^{-2}) along isopycnal 27.60 kg/m^3 with superimposed contours showing anticyclonic (A_{DCV_s}, in blue) and cyclonic (C_{DCV_s}, in red) DCVs detected by the *py-eddy-tracker* algorithm. Only DCVs with a lifetime > 21 days are shown. The solid contours define DCVs with radius $r > 15$ km and Rossby number $Ro > 0.1$; and the dashed contours define DCVs with $r < 15$ km or $Ro < 0.1$. The overlaid black contours with grayscale are the regions where the isopycnal exists $< 10\%$ in the simulation.

for the detected anticyclonic (blue) and cyclonic (red) vortices living > 21 days (Figure 3). These contours include anticyclonic DCVs (A_{DCV_s}) and cyclonic DCVs (C_{DCV_s}) for the instance shown in Figure 2b. The algorithm detects most of the DCVs that are visible to the eye.

2.6 Eddy filtering

We apply criteria based on radius (r) and Rossby number ($Ro = U/(f \times r)$), where U is the maximum radial velocity, and f is the Coriolis parameter, to the detected eddies to isolate the large and energetic ones (distinguished by solid and dashed contours in Figure 3). The smallest eddies that the algorithm can detect have a radius of about 5 km. However, we cannot trust the realism of eddies smaller than the effective resolution of the model $5 \times \Delta x = 15$ km, where $\Delta x = 3$ km, the horizontal resolution of the model. We also choose to discard the less energetic eddies, with $Ro < 0.1$. This combination of constraints, $r > 15$ km and $Ro > 0.1$, must be satisfied for at least half of the lifetime of the eddies to qualify them. The full distribution of DCVs in Ro and r is shown in the Appendix A (Figure 18). Thus, the small and less energetic eddies are filtered out and only the large and energetic DCVs are retained in the following analysis (unless otherwise stated).

3 Results

The following sections present a detailed analysis of the detection of DCVs and their life cycle. In Section 3.1, we present the statistical analysis of the DCVs in the NEA and in Section 3.2 the life cycle of $A_{meddies}$ and their interactions with other DCVs. We discuss the generation mechanisms of $A_{meddies}$ and $C_{meddies}$ and their growth in Section 3.2.1. Section 3.2.2 explains why there are so few long-lived $C_{meddies}$. Next, we present examples of interactions between A_{meddy} and several other types of eddies, including an anticyclonic eddy containing AAIW (A_{aaiw}) in Section 3.2.4.1, C_{DCV_s} generated near the African coast south of 30°N in Section 3.2.4.2, and a Canary A_{DCV} (A_{canary}) in Section 3.2.4.3. Finally, we describe the disappearance of A_{meddy} in Section 3.2.4.4.

3.1 Statistics

The distribution of C_{DCV_s} and A_{DCV_s} living for at least for 21 days along the isopycnal 27.60 kg/m^3 is shown in Figure 4. We detect an average of 609.36 C_{DCV_s} and 637.04 A_{DCV_s} contours at any given time over the area shown in Figure 4a, considering all DCVs that live at least 21 days, without the filtering based on radius (r) and Rossby number (Ro). This means that 51.11% of the detected contours are A_{DCV_s} and 48.89% are C_{DCV_s}. They correspond to $32,800$ ($36,776$) A_{DCV_s} (C_{DCV_s}) tracks having a minimum lifetime of 21 days, i.e., 47.14% of the tracks are anticyclonic and 52.86% are cyclonic. As an immediate consequence, we can state that A_{DCV_s} live longer (on an average) than C_{DCV_s}. Areas close to the boundaries created by continental shelves, islands, and seamounts have the highest number of detections compared to the rest of the ocean, with at least one detection per degree squared at any given time. There is a slight dominance of the C_{DCV_s} near boundaries, with no clear polarity bias in the open ocean (Figure 4c). However, most of the DCVs detected near the boundaries have a radius smaller than 15 km and $Ro < 0.1$.

Once we filter the distribution to keep only the large and energetic vortices ($r > 15$ km and $Ro > 0.1$ for at least half of their lifetime). The number of detections decreases to 99.16 C_{DCV_s} and 168.8 A_{DCV_s} at any given time (Figure 4b), corresponding to 63% of A_{DCV_s} and 37% of C_{DCV_s}. This corresponds to $4,545$ ($3,379$) A_{DCV_s} (C_{DCV_s}) tracks (lifetime > 21 days), i.e., 57.36% of the tracks are anticyclonic and 42.64% are cyclonic. The regions with the highest number of detections are still near the boundaries, with almost one detection per degree squared at any given time. In contrast, the open ocean has much less than one detection per degree squared at any given time (Figure 4b). There is a clear dominance of the A_{DCV_s} over the entire basin with a slight dominance of the C_{DCV_s} only very close to boundaries (Figure 4d), when considering only the large and energetic vortices.

We can estimate the probability of finding an A_{DCV} at each location by computing the fraction of the area covered by A_{DCV_s} on average within each bin (Appendix A, Figure 19). Considering only the energetic A_{DCV_s}, we find a high probability (up to $6-10$%) near

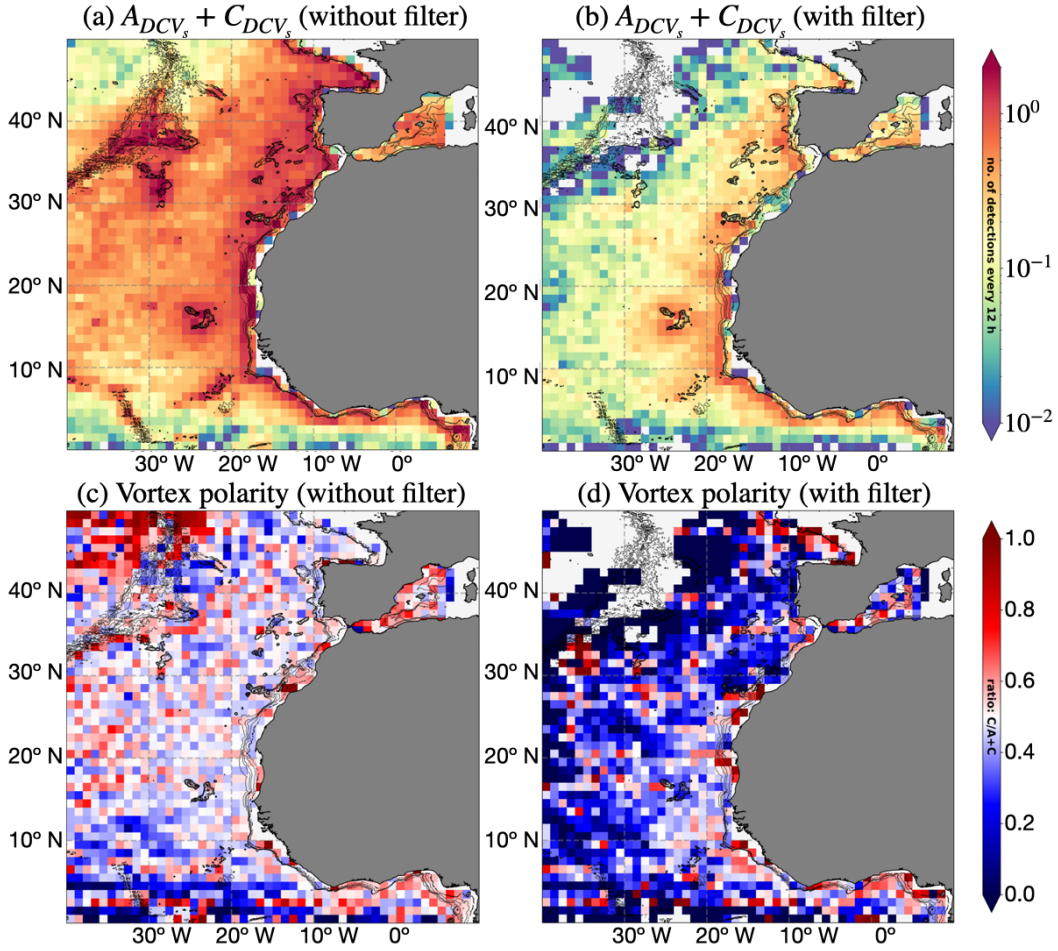

Figure 4. Distribution of the DCVs with a lifetime of at least 21 days. Number of detections (per 12 hours and per degree-squared) and eddy polarity for (a, c) the unfiltered distribution, and (b, d) the filtered distribution. The filtered distribution refers to the tracks with radius, $r > 15$ km and Rossby number, $Ro > 0.1$ for at least half of their lifetime. The eddy polarity is calculated as $C_{DCV_s}/(C_{DCV_s} + A_{DCV_s})$. Red indicates a dominance of the C_{DCV_s} and blue indicates a dominance of the A_{DCV_s}. The superimposed black contours are isobaths at 2000 m, 2500 m, 2700, and 3000 m.

the coast, decreasing to about $\sim 1\%$ away from the boundaries. These probabilities are consistent with observational results using Argo vertical profiles, which find probabilities of about $\sim 1-2\%$ in the NEA, with higher probabilities near the coast (Figure 10, McCoy et al., 2020). Although, there are obvious differences between the two methods, as we include structures without strong T/S anomalies, which would not be detected by the algorithm of McCoy et al. (2020), and consider the whole vortex area, even if a possible anomaly would not be detectabale close to the edge.

The distribution of radii (Figure 5a-b) confirms the dominance of the A_{DCV_s} for $r > 20$ km and the dominance of the C_{DCV_s} for $r < 15$ km, and about equal numbers of A_{DCV_s} and C_{DCV_s} for r between 15 and 20 km. The distribution of velocities (Figure 5c-d) shows that the ratio of A_{DCV_s} and C_{DCV_s} is close to unity for $v \in [0; 0.2]$ m/s, but the A_{DCV_s} dominate for rotational velocities $v > 15$ cm/s. Thus, the fast rotating and large DCVs are predominantly anticyclonic (Figure 5c, d), while the small ones are cyclonic.

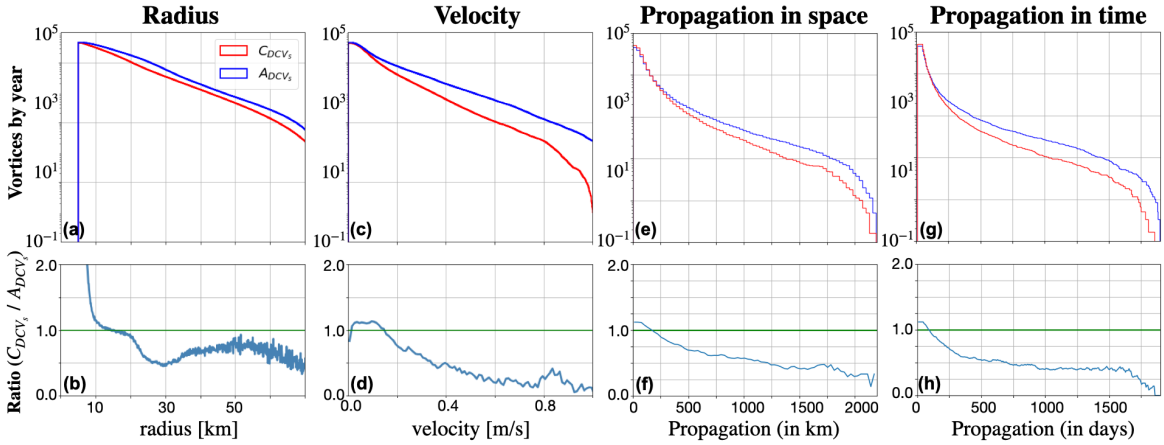

Figure 5. Cumulative distribution of detections per year (1st row) and ratio between the C_{DCV_s} and the A_{DCV_s} (2nd row) for (a, b) radius (in km); (c, d) velocity (in m/s); (e, f) propagation in space (in km); and (g, h) propagation in time (in days). The red and blue curves represent C_{DCV_s} and A_{DCV_s} respectively.

Next, we consider a possible parity bias in the eddy propagation. The DCVs that travel distances less than 2300 km and survive less than 100 days are mainly C_{DCV_s}, while the DCVs that travel longer distances ($>$ 2300 km) and survive longer ($>$ 100 days) are mainly A_{DCV_s} (Figure 5e-h). Thus, anticyclones dominate among the long-lived and long-distance DCVs. On the contrary, the C_{DCV_s} are mostly short-lived and travel shorter distances.

In the NEA region considered here, over a period of 7 years, we detect 70 A_{DCV_s} tracks and 33 C_{DCV_s} tracks persisting longer than 730 days, i.e. 68% of the very long-lived tracks are A_{DCV_s}. These very long-lived DCVs are mainly generated along the European and the African continental slopes (Figure 6). C_{DCV_s} propagate poleward (northwestward) and A_{DCV_s} propagate equatorward (southwestward) under the influence of the $\beta-$effect. A few selected long-lived tracks of DCVs from Figure 6 are discussed in detail in the next section (Section 3.2). These include A_{meddy}, A_{aaiw}, A_{canary}, and $C_{african}$.

3.2 Meddies: life cycle and interactions

3.2.1 Generation and growth of meddies

Meddies are defined here as the eddies generated in the geographical region: $35° - 40°$N, $11° - 6°$W. The current that gives birth to them at this depth is the MW outflow. The MW outflow enters the NEA through the Strait of Gibraltar and then flows northwest towards the Portimao Canyon in the Gulf of Cádiz, veering north at the Cape St. Vincent. The MW outflow is visible as a strip of positive normalised vorticity, ζ/f and positive salinity anomaly ($S \sim 36.5$ g/kg) on the continental slopes of Spain and Portugal (Figure 3). The positive vorticity is partly due to the stretching of the MW outflow, after it exits the Strait of Gibraltar. Positive vorticity also results (locally) from the MW outflow descending in canyons. Negative vorticity, on the other hand, is created by water climbing back up the continental slope and by frictional effects along the continental slope. Meddies are generated by several processes involving flow instabilities and interactions of the current with capes and canyons (D'Asaro, 1988a; Chérubin et al., 2000, 2007).

In our simulation, meddies are generated all along the Iberian slope in the Gulf of Cádiz, at the Cape St. Vincent and further north near the Setubal Canyon and the Estremadura Promontory, as shown in Figure 7c, d, in agreement with previous numerical studies (cf.

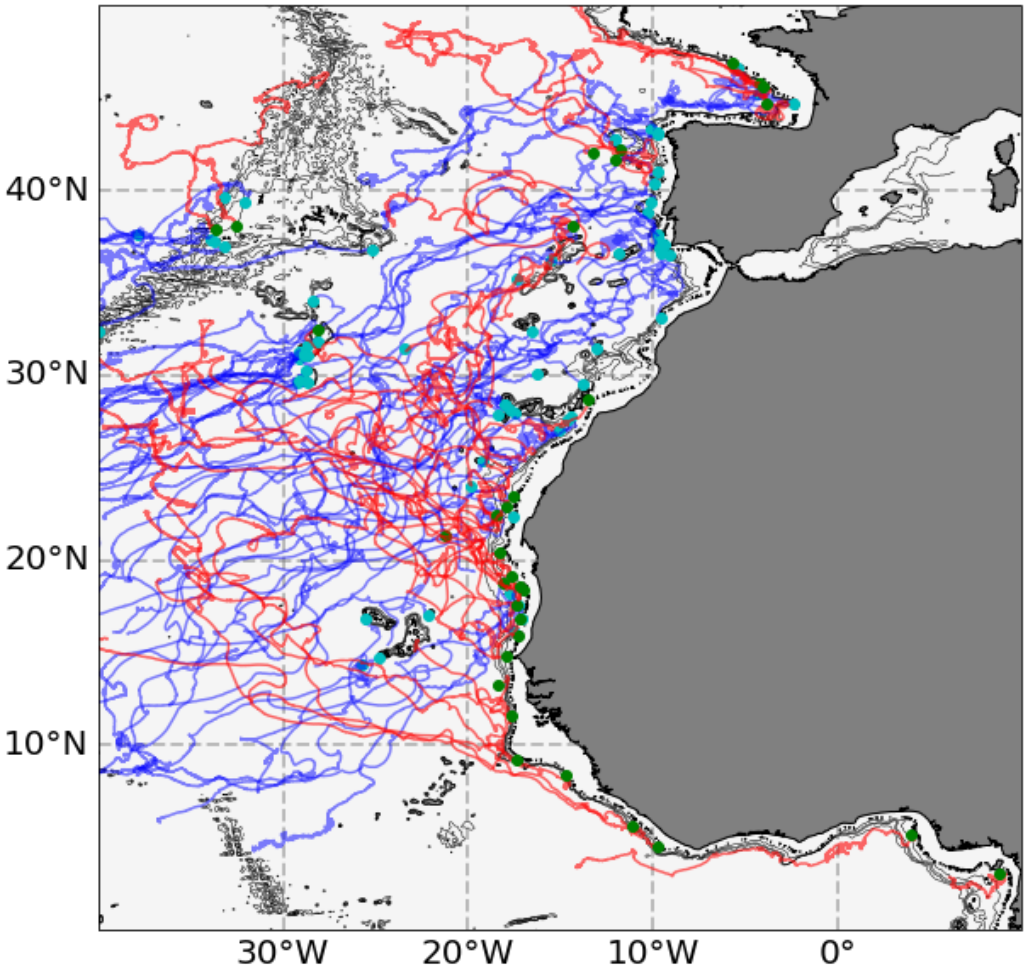

Figure 6. Trajectories of the DCVs living more than 730 days along the isopycnal 27.60 kg/m^3. The A_{DCV_s} tracks are shown in blue and the C_{DCV_s} tracks are shown in red. The cyan and green dots indicate the origin of the A_{DCV_s} and the C_{DCV_s} tracks, respectively. The overlaid black contours with grayscale are the regions where the isopycnal exists $< 10\%$ in the simulation. The superimposed black contours are isobaths at 2000 m, 2500 m, 2700, and 3000 m.

Aguiar et al., 2013). The $A_{meddies}$ originate predominantly from Cape St. Vincent (Figure 7d), where the outflow often detaches from the slope. The $C_{meddies}$ are generated more uniformly along the southern slope in the Gulf of Cádiz and along the western slope downstream from Cape St. Vincent (Figure 7c).

The $A_{meddies}$ then grow in size by repeatedly merging with other meddies of the same polarity. The small, newly formed $A_{meddies}$ tend to merge or be absorbed by larger $A_{meddies}$ in the vicinity of the Cape St. Vincent. A typical merging event between two $A_{meddies}$ is shown in Figure 8. The large A_{meddy} ($r = 26.7$ km and $v = 0.39$ m/s) absorbs the small A_{meddy} ($r = 17.3$ km and $v = 0.38$ m/s) (Figure 8a) to form a larger and more energetic A_{meddy} ($r = 30.5$ km and $v = 0.42$ m/s, Figure 8f). The larger A_{meddy} experiences an increase of 3.8 km in its r and 0.03 m/s in its v during the merger.

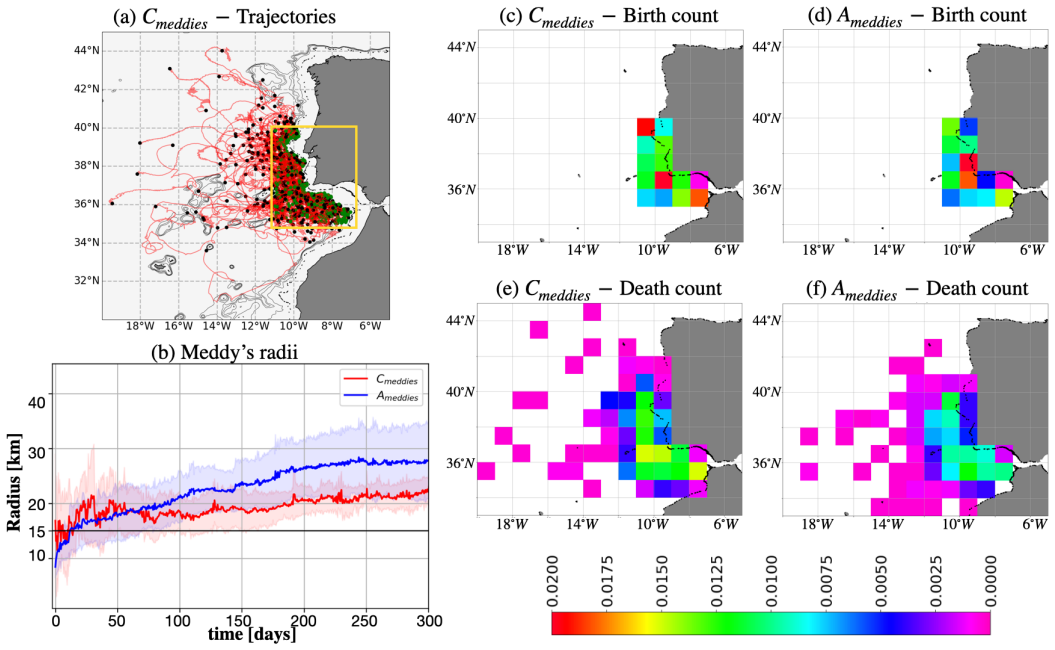

Figure 7. (a) Trajectories of the cyclonic meddies living longer than 21 days (meddies are defined here using the geographic criterion, corresponding to the yellow box); green and black dots represent cyclonic meddy generation and destruction sites, respectively. (b) Mean radii (in km), cyclonic (anticyclonic) meddies in red (blue) living longer than 365 days; the shaded region denotes the standard deviation for the cyclonic (anticyclonic) meddies. Birth and death count of the cyclonic (c, e) and the anticyclonic (d, f) meddies, respectively, living longer than 21 days, in $1^\circ \times 1^\circ$ bins. The maps are shown along isopycnal 27.60 kg/m^3. The contour lines in black denote where the isopycnal exists $< 10\%$ in the simulation.

The evolution of the radii of the meddies (including only those that live longer than 365 days) is shown in Figure 7c. While the mean radii are initially around 10 km for both $C_{meddies}$ and $A_{meddies}$, they grow steadily over weeks for $C_{meddies}$ and months for $A_{meddies}$ to reach 20 km and 30 km, respectively.

The $A_{meddies}$ produced southwest of the Iberian Peninsula often end up forming fairly stationary large $A_{meddies}$ due to these successive mergers (Movie 01, `https://vimeo.com/829308815`). One of these stationary $A_{meddies}$ is visible at 37.5°N, 12°W in Figure 3. These large $A_{meddies}$ are trapped by the Horseshoe Seamounts in the south (in particular the Josephine and Gorringe bank, Figure 1) and recirculate anticyclonically around the Tagus Abyssal Plain. The Tagus Abyssal Plain has the form of a bowl, which is known to promote the formation and trapping of anticyclonic eddies (de Marez et al., 2021; Solodoch et al., 2021).

3.2.2 Why are there only a few long-lived $C_{meddies}$?

The $C_{meddies}$ tend to be destroyed closer to their generation sites than the $A_{meddies}$. The main sites of destruction for $C_{meddies}$ and $A_{meddies}$ are shown in Figure 7e, f. Most of the events are concentrated in the region defined inside the yellow box in Figure 7a. 36.36% of $A_{meddies}$ are able to escape this region, while only 26.93% of $C_{meddies}$ are able to do so. This means that the $C_{meddies}$ are unable to travel as far as the $A_{meddies}$ and die on an average closer to where they were created.

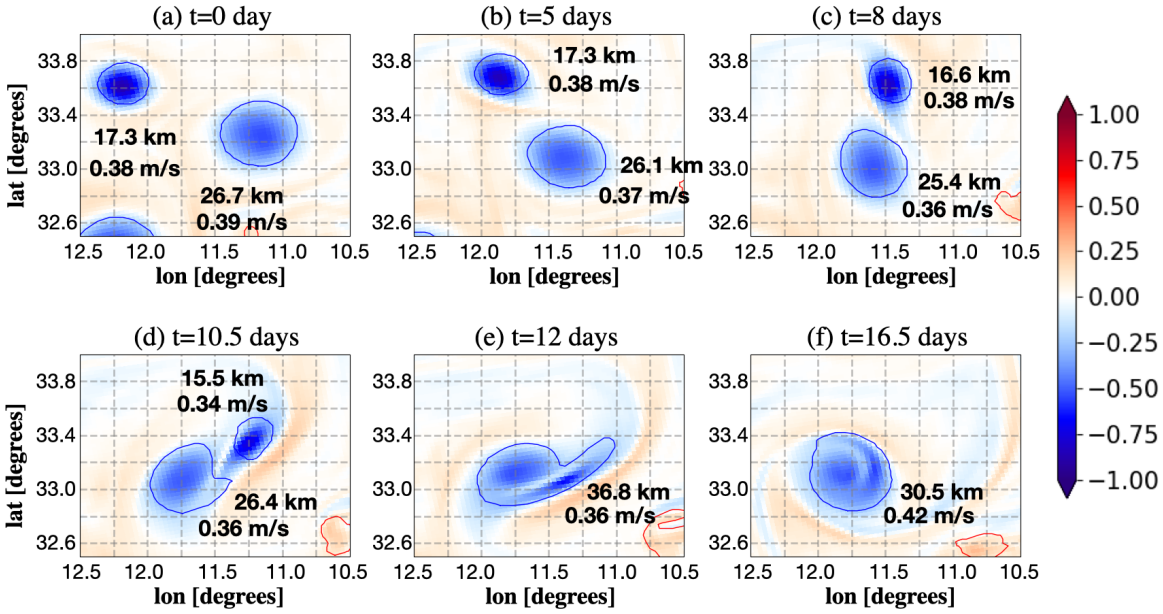

Figure 8. Merging event between two $A_{meddies}$. The colorscale shows the relative vorticity (ζ/f) along the isopycnal 27.60 kg/m^3. The blue and red contours indicate the detected anticyclones and cyclones. The radii (in km) and maximum radial velocities (in m/s) of the anticyclones are given in the figure.

These destructions can be caused by the meddies being either absorbed by meddies of the same polarity, as previously shown in Figure 8, or destroyed by a meddy of the opposite polarity. An example of a C_{meddy} being destroyed by an A_{meddy} is shown in Figure 9. As the C_{meddy} comes close to the (larger) A_{meddy}, it is strained by the anticyclonic flow and forms a filament of cyclonic vorticity (Figure 9b). Then as the filament rolls up around the A_{meddy}, it ends up forming a cyclonic shield around the A_{meddy} (Figure 9c).

The evolution of the mean radius (Figure 7b) highlights a different behavior for the $C_{meddies}$ and the $A_{meddies}$. While the $A_{meddies}$ grow steadily with time by successive mergers over several months, up to a year, the $C_{meddies}$ grow only initially over the first few weeks, but do not grow significantly after that. Previous studies of vortex merging in stratified rotating shallow-water flows (Arai & Yamagata, 1994) have shown that anticyclones tend to be larger than cyclones and merge more easily (at greater distances). This can explain the preferential growth of the $A_{meddies}$ by merger compared to the $C_{meddies}$, as seen in our simulations. As a result, the $A_{meddies}$ are larger and more energetic than the $C_{meddies}$. Thus, the $A_{meddies}$ create a strong deformation field around them, leading to the destruction of the $C_{meddies}$ by stretching and shearing. The $C_{meddies}$ then decay into filaments (Figure 9b) and/or wrap around the $A_{meddies}$ forming a vorticity shield (Figure 9c).

We thus explain the shorter lifespan of the $C_{meddies}$ by the destructive presence of strong and energetic $A_{meddies}$ in the vicinity of the Iberian coast. As the $C_{meddies}$ drift northwestwards under the influence of the $\beta-$effect, they are often destroyed near the Cape St. Vincent where the strong, almost stationary, $A_{meddies}$ are sitting. The trapping of the $C_{meddies}$ in the Horseshoe Basin and the continental slope near the Gulf of Cádiz affects the trajectories of the $C_{meddies}$ and their termination. In contrast, the long-lived $C_{meddies}$ that can survive for more than 730 days are found north of 40°N (Figure 6), and are thus distant from the strong anticyclonic field.

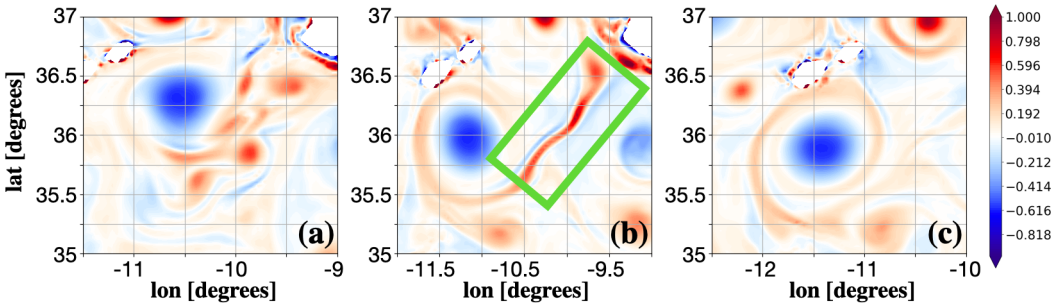

Figure 9. Horizontal maps of vorticity (ζ/f) along the isopycnal 27.60 kg/m^3 (a) $t = 0$, before the destruction of the cyclonic meddy (C_{meddy}) as it is strained by an anticyclonic meddy (A_{meddy}); (b) filament formation after $t = 14.5$ days, highlighted with green box; and (c) a shield around the A_{meddy} after $t = 20$ days.

3.2.3 Meddies propagation

Eighteen $A_{meddies}$ with lifetimes > 365 days are generated during the simulation (including only those whose entire lifetime is included in the simulation). Of these $A_{meddies}$, five decay in the region $35° - 40°$N, $11° - 6°$W, i.e., they stay close to their generation site without propagating further south. The other thirteen $A_{meddies}$ propagate outside of this domain. The time evolution of the radius of the thirteen $A_{meddies}$ and their composite is shown in Figure 10b, c, for the first 500 days of their life. The $A_{meddies}$ undergo several merging events near the Gulf of Cádiz and the Cape St. Vincent in the first few months after their generation, as seen previously. This growth phase occurs preferentially near the generation sites, when the spatial density of the eddies is greatest. The radii of the $A_{meddies}$ become larger than 15 km during the first 50 days and grow steadily during the first 250 days to reach radii between 20 and 45 km (Figure 10b, c). After 250 days, the radii of the different $A_{meddies}$ are more stable, with the exception of A_{meddy} 11 (between $350 - 450$ days), which undergoes a large increase in radius due to merging with A_{meddy} 04.

Most of the long-lived $A_{meddies}$ (03, 04, 05, 06, 07, 09, 10, and 11 in Figure 10) are first detected downstream of Cape St. Vincent, along the southwestern Iberian slope. They then propagate westward, between $38° - 40°$N, until they veer southwestward west of 20°W. This corresponds to the *highway* described in Aguiar et al. (2013). Among them, A_{meddy} 05 and 10 are typical examples of meddies that remain trapped for some time north of the Horseshoe Seamounts (Figure 1), where they grow by merging with the smaller $A_{meddies}$ formed along the southwestern Iberian slope. They then escape and propagate farther away until they are finally destroyed by colliding with seamounts around 32°N, 37°W.

A_{meddy} 01, 02, 08, 12 and 13 have trajectories starting south of the other meddies, corresponding to the *winding path* mentioned in Aguiar et al. (2013). A_{meddy} 01 goes directly through the Horseshoe Seamounts, between the Ampère and Gorringe Bank Seamounts, and then continues west to 20°W. A_{meddy} 02 initially propagates straight south, bypassing the Horseshoe Seamounts and the Madeira Island from the south, and then propagates southwest until 25°W, where it veers south (Figure 10a). Of the thirteen $A_{meddies}$, only A_{meddy} 08 is able to cross the Mid-Atlantic Ridge (MAR). A_{meddy} 07 can get close to the MAR, but it shears its core at 19.2°N, 43.4°W after travelling a distance of 6347.07 km. A_{meddy} 08 crosses the MAR at about 17°N before its core is destroyed after travelling a total of 10,683.52 km in 2120.5 days (5.81 years) with a salinity of about 35.3 g/kg at 16°N, 49.7°W.

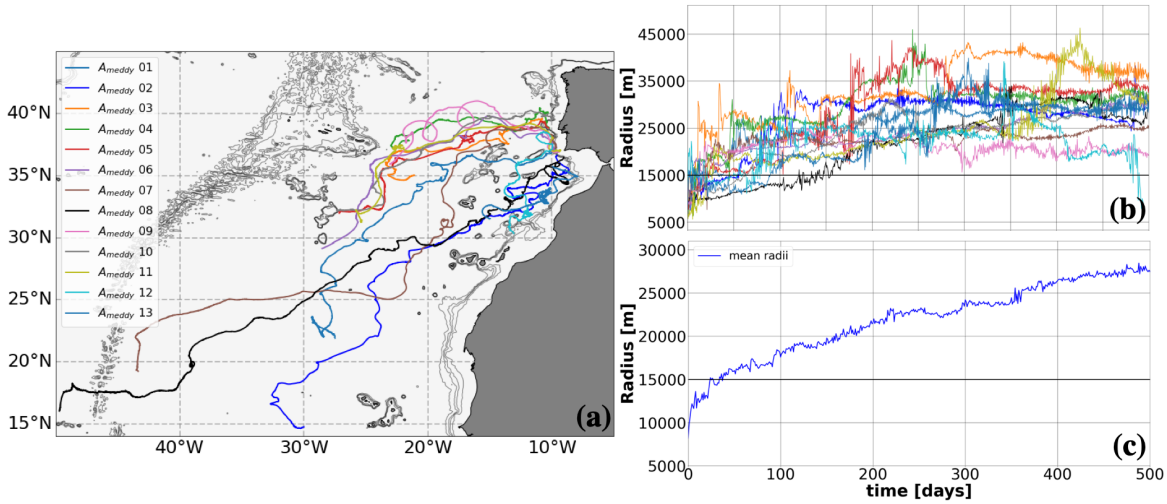

Figure 10. (a) Trajectories of the anticyclonic meddies ($A_{meddies}$) living > 365 days. Radius (in m) w.r.t. time (in days) for 13 $A_{meddies}$: (b) trajectory of individual radius; (c) mean radii. The maps are shown along isopycnal 27.60 kg/m^3. The superimposed black contours in (a) are isobaths at 2000 m, 2500 m, 2700, and 3000 m.

3.2.4 Interactions between meddies and other DCVs

The $A_{meddies}$ undergo many interactions with neighboring eddies during their lifetime. Interactions are considered here when the distance between two DCVs is less than a quarter degree. These interactions can lead to change in: radius, velocity, direction of propagation, salinity, and/or temperature inside the core of the vortex, and can lead to the formation of vortex dipoles or tripoles. An example of an A_{meddy} undergoing multiple interactions with A_{aaiw}, A_{canary}, and $C_{african}$ is shown in Figure 11a and discussed in this section. It corresponds to the A_{meddy} 02 in Figure 10a). This particular A_{meddy} is chosen to illustrate the richness of the interactions of the $A_{meddies}$; it is not an exceptional case. Many $A_{meddies}$ experience multiple interactions along their path, especially as they drift southwest in the Canary/Cape Verde basins.

The A_{meddy} shown in Figure 11a is generated at the mouth of the Gulf of Cádiz (at 36.61°N, 9.58°W) near Cape St. Vincent. Its horizontal and vertical extent are shown 62.5 days after its formation in Figure 12. The meddy core lies between 1000 and 1500 m on the σ = 27.60 kg/m^3 isopycnal surface (Figure 12b). The growth of this A_{meddy} is the result of multiple merging events occurring during the first 150 days (Figure 11d). The strongest merging event (in terms of radial variation) that occurs during the lifetime of this A_{meddy} corresponds to the one shown previously in Figure 8. It is marked as ⓘⓘ with a black circle in Figure 11.

The markings in Figure 11 highlight the coexistence (in blue) and/or interactions (in red) of the A_{meddy} with nearby vortices: A_{aaiw}, A_{canary}, and $C_{african}$. In addition, the time series of salinity, change in trajectory angle, radius, and velocity of the A_{meddy} are shown in Figure 11b-e, along with A_{meddy} related events marked with numbers.

3.2.4.1 Co-existence of A_{meddy} and A_{aaiw}

The A_{aaiw} is an anticyclone containing AAIW in its core (Section 2.2 and Figure 2c). It is generated near the Moroccan coast (34.17°N, 8.48°W). The current here comes from

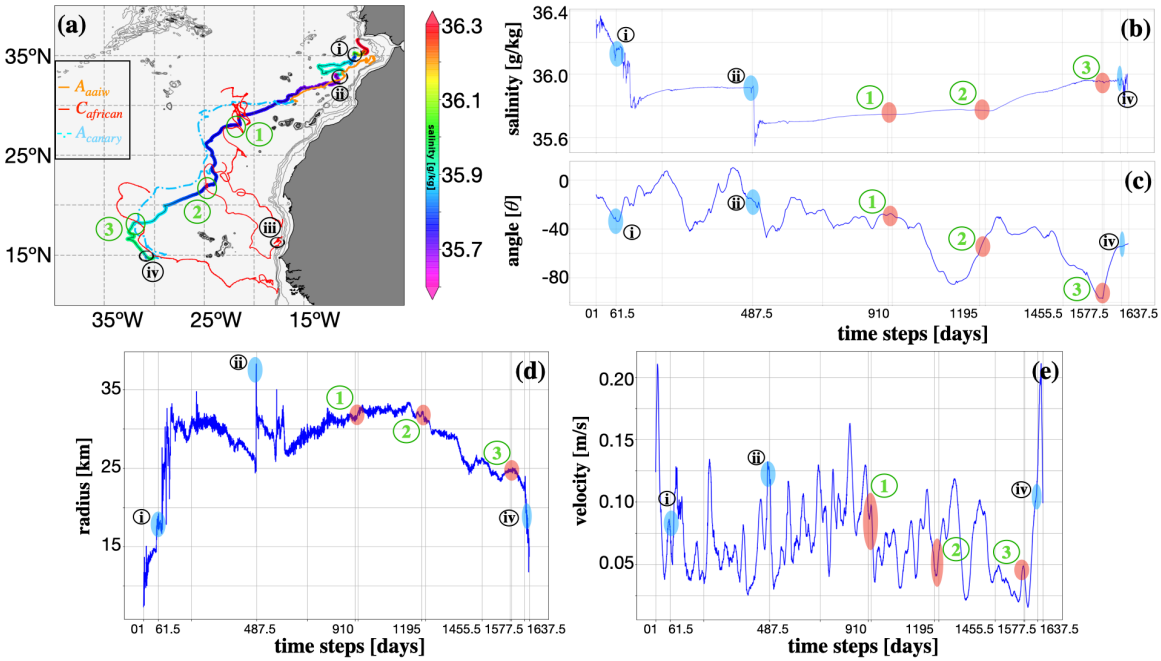

Figure 11. (a) Trajectory of a long-lived anticyclonic meddy (A_{meddy}, with salinity (in g/kg) in rainbow colors), and other DCVs interacting with it along isopycnal 27.60 kg/m^3: an A_{DCV} containing AAIW (A_{aaiw}, orange), three African C_{DCVs} ($C_{african}$, red), and a Canary A_{DCV} (A_{canary}, cyan). Time-series of the A_{meddy} are shown in terms of: (b) salinity in g/kg, (c) angle of the trajectory relative to west, (d) radius in km, (e) velocity in m/s. The numbering (①, ②, and ③) in green denotes the interaction of the A_{meddy} with the $C_{african}$ (also highlighted in red (b-e)). The numbering in black indicates the position in space and time of some typical events: ⓘ close to the A_{meddy} generation, ⓘⓘ largest merging event of the A_{meddy}, ⓘⓘⓘ close to the $C_{african}$ generation, and ⓘⓥ just before the destruction of the A_{meddy}. ⓘ, ⓘⓘ, and ⓘⓥ events are highlighted in blue; and ①, ②, and ③ events are highlighted in red in the time-series (b-e). The contour lines in (a) denote the topography at 100 m, 1000 m, 1500 m, 2000 m depth.

the south along the African coast towards the Gulf of Cádiz at a depth of 1000 m. The two anticyclones, A_{meddy} and A_{aaiw}, travelled for 442.5 days and 500 days, respectively, before the encounter. They meet near $31° - 35°$N, $14° - 10°$W, and their interaction lasts for 40 days. This co-existence is shown in Figure 13. A_{aaiw} has a larger radius than the A_{meddy}. The former extends vertically from 250 m to 2500 m depth while the latter is contained between $800 - 1800$ m depth. It should also be noted that the A_{meddy} contains warm and salty water while the A_{aaiw} contains fresher and colder water.

The presence of the A_{aaiw} affects the drift of the A_{meddy} (Figure 11a) and explains the change in the angle of the A_{meddy} trajectory. This coexistence does not lead to any major change in the radius and velocity of the A_{meddy}. Finally, the A_{aaiw} lives for 668 days and travels a distance of 2090.89 km, averaging 1.98 km per day, before being destroyed at 30.42°N, 15.69°W after hitting a seamount.

3.2.4.2 Interaction of A_{meddy} with $C_{african}$ south of 30°N

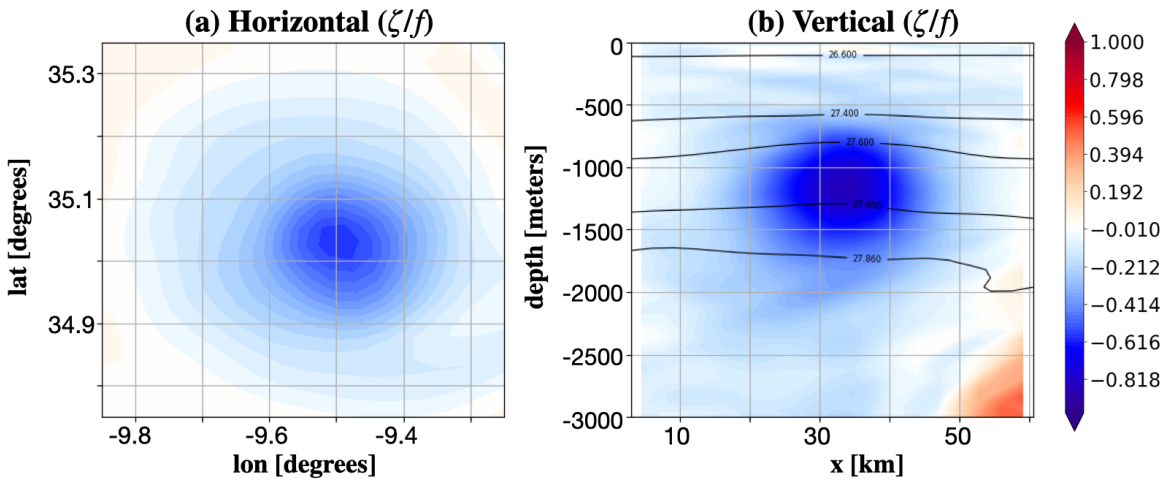

Figure 12. Snapshots of ζ/f 62.5 days after the A_{meddy} generation (a) along isopycnal 27.60 kg/m^3 and (b) vertical section along 9.5°W. Black contours in (b) are isopycnals in kg/m^3.

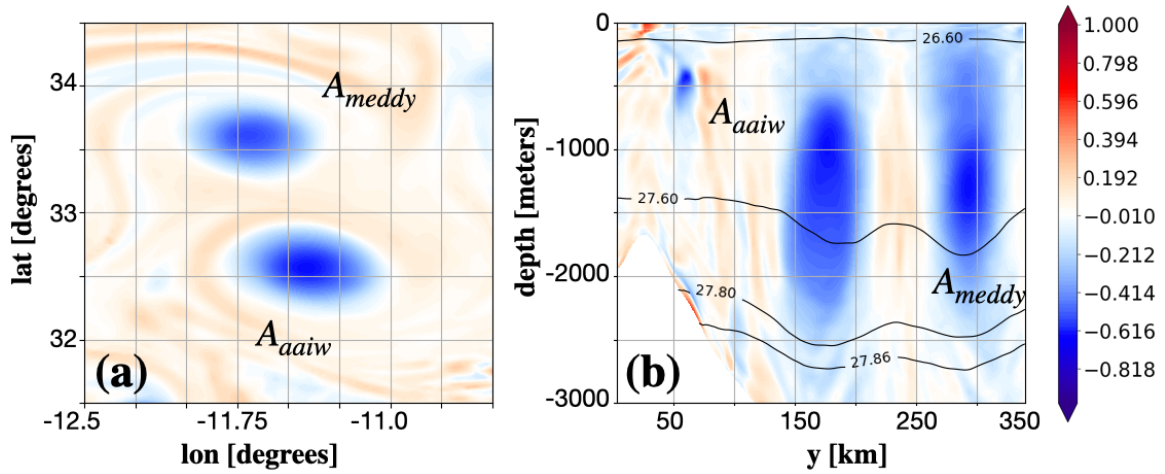

Figure 13. The co-existence of the A_{aaiw} and the A_{meddy} with maps of ζ/f (a) along isopycnal 27.60 kg/m^3, and (b) in the vertical. Black contours in (b) are isopycnals in kg/m^3.

Many C_{DCV_s} are generated along the African coast, south of 30°N. They are called $C_{african}$ here. Some of them can be very long-lived, as shown in Figure 6. This section presents the interaction of the A_{meddy} with the three $C_{african}$ shown in Figure 11.

An overview of the evolution of the $C_{african}$ is the following:

1. The long-lived $C_{african}$ generated south of 5°N remain in the vicinity of the African continental shelf and do not move offshore. Their proximity to the coast generates a mirror-effect (the flow field mirrors into the wall) that drives them westward (along the zonal coast) (X. Carton et al., 2013). This effect combines with the $\beta-$drift, which advects cyclones northwestward. Thus, these $C_{african}$ do not leave the continental slope.
2. North of 5°N, the African coastline's orientation gradually changes to become more meridional. Then, the $C_{african}$ generated along the African coast propagate northward by the mirror-effect and northwestward by the $\beta-$drift. They can thus detach

from the coast. This is observed in particular at capes, which help the eddy detachment process. Once detached, these deep cyclones can interact with the $A_{meddies}$ in the open ocean.

We now select the three $C_{african}$ interacting with the A_{meddy} (Figure 11) and study them in detail. The $C_{african}$ are generated by the interactions of southward flowing currents with the African continental slope. Friction acts on currents to form a frictional boundary layer, which detaches near capes, becomes unstable, fragments and rolls up to form (D'Asaro, 1988a; Srinivasan et al., 2019). The generation of $C_{african}$② is illustrated in Figure 14. The four moments correspond to: three days before the first detection of $C_{african}$② (Figure 14a); the moment it is first detected (Figure 14b); three days later (Figure 14c); and when it is fully developed (129 days after the first detection, Figure 14d) with a radius $r = 18.8$ km and $v = 0.42$ m/s. In the first three stages, the cyclone is formed by the fragmentation and roll-up of the shear layer. Its further growth is due to the merger of various patches of cyclonic vorticity. The generation of $C_{african}$③ with snapshots of horizontal and vertical maps of ζ/f, and vertical maps of potential vorticity (PV) is presented in the Appendix A (Figure 21).

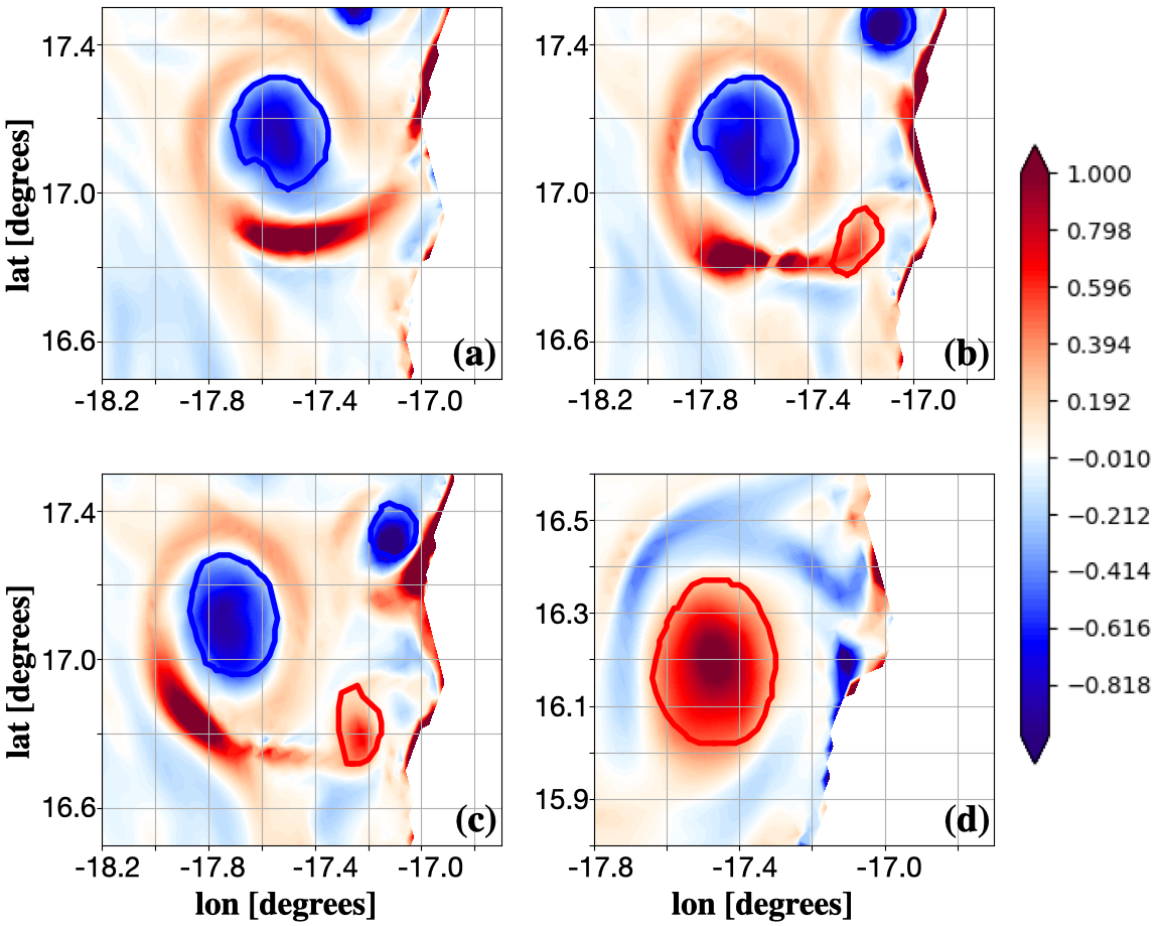

Figure 14. Successive snapshots of ζ/f along isopycnal 27.60 kg/m^3 showing $C_{african}$②: (a) three days before the generation of $C_{african}$②, (b) generation of $C_{african}$②, (c) three days after the generation, and (d) 129 days after the generation. Superimposed contours show anticyclonic (in blue) and cyclonic (in red) DCVs detected by the *py-eddy-tracker* algorithm.

The long-lived A_{meddy} generated at the mouth of the Gulf of Cádiz (Section 3.2.1) interacts with the three long-lived $C_{african}$ throughout its lifetime of 1660 days. These interactions are highlighted in space by green circles, with the numbers referring to the order of interaction in Figure 11a. The first interaction of the A_{meddy} takes place after 910 days and the last interaction takes place after 1577.5 days. These interactions lead to the formation of transient vortex dipoles (pairing of the A_{meddy} with each $C_{african}$), which result in an acceleration of the A_{meddy} drift with slight changes in its strength. Furthermore, these interactions are fairly short: the longest one is the interaction with $C_{african}$②, which lasts 18 days.

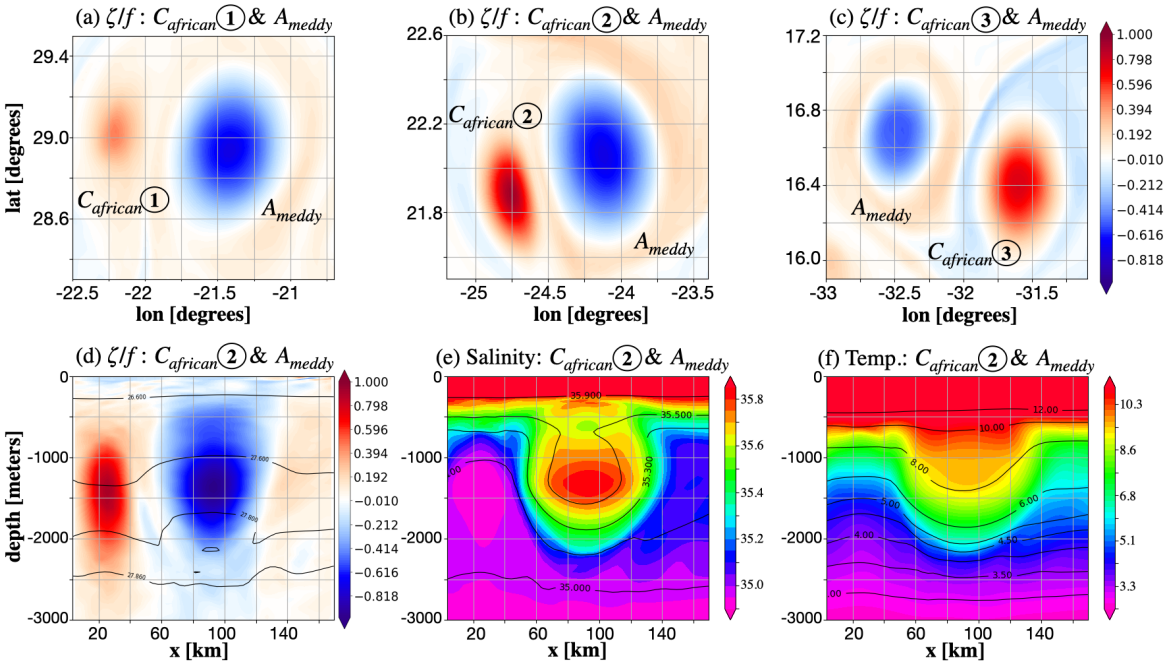

Figure 15. (a-c) Maps of ζ/f along isopycnal 27.60 kg/m^3 showing dipoles formed by A_{meddy} and: (a) $C_{african}$①, (b) $C_{african}$②, and (c) $C_{african}$③. (d-f) vertical maps of ζ/f, salinity (in g/kg), and temperature (in °C) for $C_{african}$② with overlaid contours of isopycnals, isohalines, and isotherms, respectively. The three snapshots shown are at 912.5 days, 1205.5 days, and 1577.5 days after the A_{meddy} generation.

These three cyclones (denoted $C_{african}$①, $C_{african}$②, and $C_{african}$③ in Figure 11a) are shown in Figure 15. Their core lies at 1500 m. The three snapshots shown correspond to times of 912.5 days, 1205.5 days, and 1577.5 days after A_{meddy} generation (Figure 11 and 15). $C_{african}$② is chosen to show a typical vertical extension of the $C_{african}$; their vertical structures in vorticity (ζ/f) are fairly similar; their salinity and temperature are close to 34.9 g/kg and 4°C, respectively. After its interactions with the $C_{african}$, the thermohaline properties of A_{meddy} do not change significantly and remain close to 9.93°C and 35.8 g/kg. The changes in radius and velocity are also negligible for the three interactions. Concerning the $C_{african}$, the largest change in radius occurs for $C_{african}$①; it is smaller for $C_{african}$②, and the core of $C_{african}$③ has no change in radius. This difference in the strength of the interaction with the $C_{african}$ is due to the absence (Figure 15a) or to the presence (Figure 15c) of a vorticity shield for the different cyclones.

The three $C_{african}$ live for 1335.5 days, 744.5 days, and 803 days and travel 7999.24 km, 3274.98 km, and 4980.57 km, respectively. They do not experience the same fate as the

497 $C_{meddies}$. This can be explained by several reasons. Firstly, the $C_{african}$ have a vorticity
498 shield (for example, $C_{african}$③) which renders interactions with $A_{meddies}$ less efficient than
499 those between $A_{meddies}$ and small, newborn, $C_{meddies}$. Secondly, the population of C_{DCV_s}
500 south of 30°N is larger than that of the A_{DCV_s} (unlike north of 30°N). Therefore, C_{DCV_s}
501 can survive longer via constructive interactions (merger). This larger number of $C_{african}$ is
502 a priori due to their efficient generation process.

503 The life cycle of $C_{african}$ includes several interactions with DCVs containing different
504 water masses. Nevertheless, these interactions induce relatively small changes to these DCVs
505 in terms of their $T-S$ properties. This can be explained two ways:

506 1. because the interaction of $C_{african}$ with $A_{meddies}$ leads to a vortex dipole which mod-
507 ifies the shape of the vortices, in particular rendering them asymmetric or elliptical,
508 but does not destroy them
509 2. because in triple interactions (one $C_{african}$ with two A_{DCV_s}), the cyclone only plays
510 the role of a catalyst (a catalyst is a medium that modifies the properties of the other
511 medium without affecting its own properties) by advecting one anticyclone towards
512 the other one.
513

514 *3.2.4.3 Co-existence of A_{meddy} and A_{canary}*
515

516 The A_{canary} is generated at 30.32°N, 16.23°W (Figure 11a) and lives for 1275 days,
517 covering a distance of 5041.45 km. The A_{canary} co-exists with the A_{meddy} with which it
518 forms a vortex doublet twice during its lifetime. Nevertheless, the two vortices do not merge
519 either because they remain too far apart, or because they are embedded in opposite shear
520 or strain (Perrot & Carton, 2010). The first doublet is formed before A_{meddy} interacts with
521 $C_{african}$② and it lasts for 98.5 days (Figure 16a). The second doublet is formed before
522 the interaction with $C_{african}$③ and it lasts for 46 days. The first doublet formation is
523 illustrated with the snapshot of A_{canary} and A_{meddy} in Figure 16a (horizontal maps of vor-
524 ticity). This event takes place when the A_{canary} has lived 470 days and the A_{meddy} has
525 lived for 442.5 days. The vertical extent of the A_{canary} (Figure 16c-e), is shown in Figure
526 16a with ζ/f, salinity and temperature (Figure 16c-e). The core of the A_{canary} lies between
527 $500-2500$ m depth with salinity of 35.6 g/kg and temperature of 8°C. It must be noted that
528 this A_{canary} also undergoes a tripolar interaction with A_{meddy} and $C_{african}$② (Figure 16b).
529 This tripolar interaction takes place right after the dipolar interaction between A_{meddy} and
530 $C_{african}$② and lasts for 7 days (see the horizontal map of ζ/f in Figure 16b).
531

532 Another noteworthy vortex interaction takes place near $26° - 22°$N, 23°W. A_{meddy}
533 (25.5°N, 25°W) follows a straight (90°) southward trajectory and then undergoes a sharp
534 change in angle of $\sim 45°$ around 22°N. Southward trajectories and abrupt changes in angles
535 have previously been mentioned in observations by Armi et al. (1989), and Meddy 21 in
536 Figure 13, Richardson et al. (2000). This specific motion of the A_{meddy} is related to its
537 interaction with $C_{african}$① and $C_{african}$② (Figure 11a, c). These interactions take place
538 in particular as the A_{meddy} interacts with the A_{canary}. This leads to the formation of a
539 vortex doublet and of a vortex tripole.
540

541 *3.2.4.4 Disappearance of A_{meddy}*
542

543 The A_{meddy} shown in Figure 11a has a core salinity of 36.25 g/kg and a core tem-
544 perature of 11.7°C when generated. There is a gradual decrease in salinity as the core of
545 A_{meddy} drifts southwest. However, after drifting south of 20°N, there is a slight increase in
546 salinity along isopycnal 27.60 kg/m^3; this is due to a slight change in the vertical structure

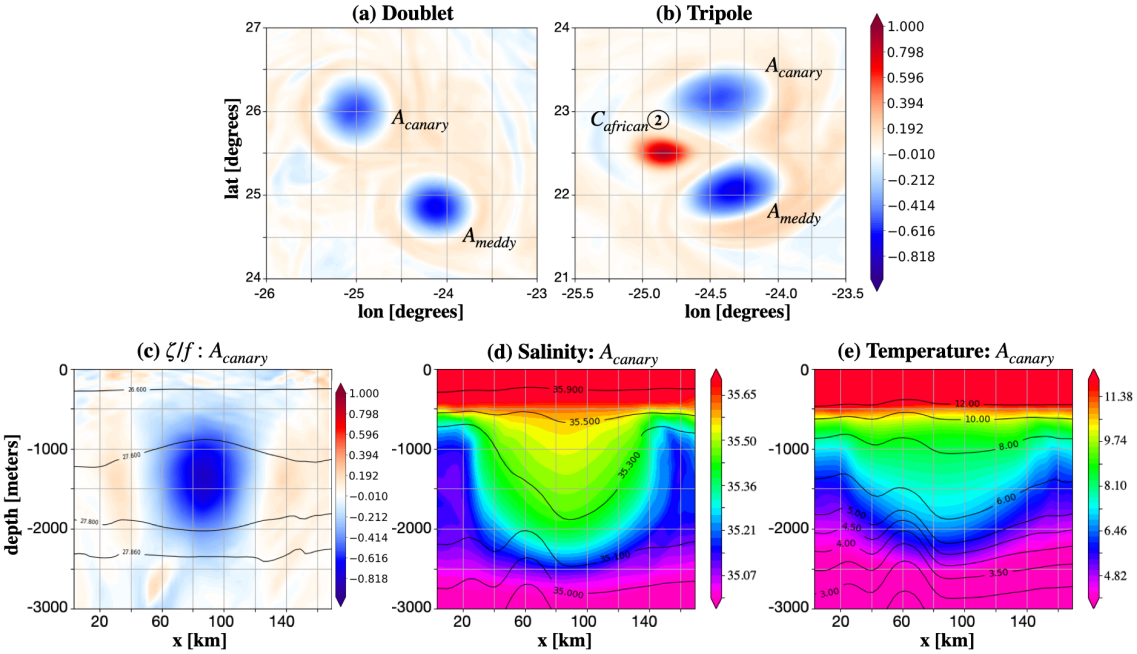

Figure 16. (a) Interaction between A_{canary} and A_{meddy}, (b) tripole formation between A_{canary}, A_{meddy}, and $C_{african}$②; along isopycnal 27.60 kg/m^3 using ζ/f. (c-e) vertical map of the instance in (a) with ζ/f, salinity (in g/kg), and temperature (in °C) respectively with their corresponding colorscale having overlaid contours of isopycnals, isohalines, and isotherms.

of the A_{meddy} with the saline core extending towards lighter densities, as shown in Appendix A. This particular A_{meddy} is not exceptional in terms of salinity increase after crossing 20°N.

At the time of the disappearance of the A_{meddy}, its core salinity is 35.94 g/kg and its temperature is 10.51°C; these values indicate a freshening ($\Delta S = 0.39$ g/kg) and a cooling ($\Delta T = 1.6$°C) of this vortex since its generation. This A_{meddy} then undergoes a slow weakening of its core before a final destruction at 14.75°N, 30°W. The destruction of the A_{meddy} is favoured by the shear flow created between A_{canary} and A_{meddy}; this shear affects the A_{meddy} during its second encounter with the A_{canary}. In total, this A_{meddy} has travelled for 1661 days and it has covered a distance of 7249.51 km, travelling 2.18 km per day. A snapshot of the A_{meddy} is shown in Figure 17 22.5 days before the A_{meddy} completely loses its coherence. The A_{meddy} core has then lost a substantial fraction of its water mass and a reduction of height to 700 m since its generation.

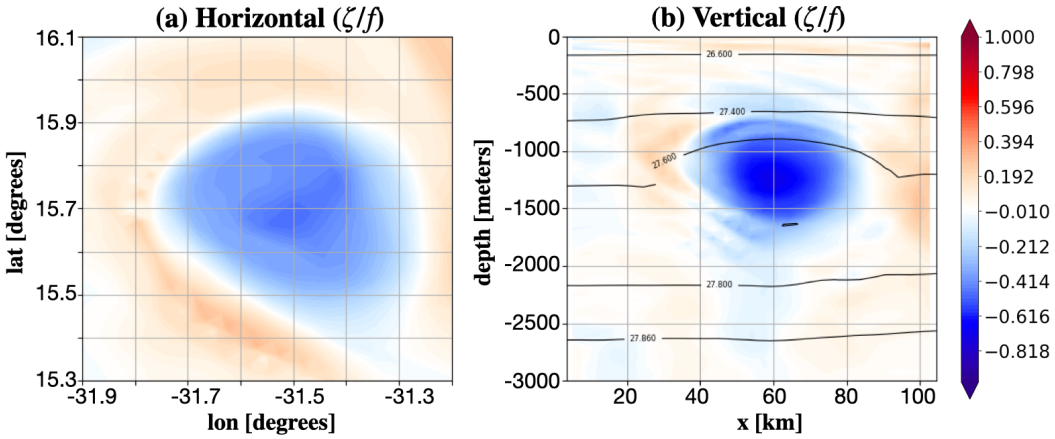

Figure 17. Snapshot of ζ/f 22.5 days before the disappearance of the A_{meddy} (a) along isopycnal 27.60 kg/m^3, and (b) along the vertical. The overlaid black contours in (b) are isopycnals.

4 Conclusion

In this study, we have presented an analysis of the life cycle of long-lived deep coherent vortices (DCVs) in the Northeast Atlantic (NEA) Ocean using a 7-year long high resolution model simulation ($\Delta x = 3$ km). The *py-eddy-tracker* algorithm by Mason et al. (2014) is employed for the detection of DCVs. Since eddies move and transport material properties along isopycnal surfaces, we perform the detection along the isopycnal 27.60 kg/m^3, which is the one where the Mediterranean Water (MW) diffuses into the NEA. The study area covers $0° - 50°$N, $40°$W $-10°$E in the NEA and the depth of the isopycnal 27.60 kg/m^3 is between $750 - 1500$ m.

We have quantified the statistical distributions properties of DCVs in terms of their radius, rotational velocity, and propagation in space and time. The model shows evidence of a preference for small and short-lived deep cyclones; and for larger, more energetic and longer-lived deep anticyclones. This result agrees with former work by, e.g., Sangrà et al. (2009); Chelton et al. (2011).

The total number of DCVs at any given time in the NEA is 1246.4 (on the isopycnal 27.60 kg/m^3), with 609.36 C_{DCV_s} and 637.04 A_{DCV_s}. These numbers decrease to 99.16 C_{DCV_s} and 168.8 A_{DCV_s} if we keep only the large and energetic vortices ($r > 15$ km and $Ro > 0.1$ for at least half of their lifetime). Some estimates have been made previously to quantify the numbers A_{DCV_s} using in-situ measurements. The methods are usually based on the detection of lenses associated with extreme temperature and salinity anomalies in vertical hydrographic profiles. Based on the extrapolation of results for a hydrographic section, Ebbesmeyer et al. (1986) estimated the average presence of one eddy per 100 km, corresponding to a total population of between 10^3 and 10^4 deep vortices in the North Atlantic ocean. Based on the analysis of Argo vertical profiles, McCoy et al. (2020) found probabilities of about $\sim 1 - 2\%$ to sample an A_{DCV} in the NEA, with higher probabilities near the coast (Figure 10, McCoy et al., 2020). Our numbers of A_{DCV_s} are therefore consistent with these estimates, bearing in mind that we include only one isopycnal and not the full vertical column, and that our method based on the velocity field includes structures without strong T/S anomalies that would not be detected by analysis of vertical hydrographic profiles alone. A more detailed comparison would be required to understand exactly which structures can or cannot be detected by these different methods.

Concerning MW eddies (meddies), we observe generations of both cyclonic meddies ($C_{meddies}$) and anticyclonic meddies ($A_{meddies}$). Aguiar et al. (2013) mentioned $28 - 31\%$ of $C_{meddies}$ living for at least 15 days at 1000 m depth with a salinity anomaly of 0.12 psu; these values are close to our detection of $C_{meddies}$ (26.93%) crossing the box region in Figure 7. The asymmetry between cyclones and anticyclones is explained here by the ability of anticyclones to grow by merging together and to form large and energetic structures, while cyclones have more difficulty merging and are more likely to be destroyed by large anticyclones. In particular, a large A_{meddy} often resides near Cape St. Vincent, absorbing small and newly generated A_{meddy} and also exerting a destructive shear on small newly generated C_{meddy}, which drifts northwestward towards it. This northwestward drift can be attributed to the planetary $\beta-$effect and to the local currents (McWilliams, 1985; Chelton et al., 2011). This predominance of southwestward drift of the A_{meddy} has been reported before by Käse et al. (1989). Nevertheless, some $A_{meddies}$ formed near the Iberian Peninsula can be destroyed locally after colliding with the Horseshoe seamounts (Richardson et al., 2000). In a previous study, the presence of meddies has been mentioned west of the Mid-Atlantic Ridge (MAR), in the Sargasso Sea (Kostianoy & Belkin, 1989). Our model outputs indicate that there is a possibility of meddies in the Northwest Atlantic Ocean i.e., $A_{meddies}$ crossing the MAR.

A key point of this study is the analysis of multiple DCVs from various origins on 27.60 kg/m^3 isopycnal, and their successive interactions with the A_{meddy} moving south/southwest from the Gulf of Cádiz (the so-called "southern meddies" in the literature). In this study,

612 we chose to present one A_{meddy} undergoing such interactions. However, it is representative
613 of many such cases occurring in the region.
614

615 Firstly, as mentioned above, an anticyclonic DCV (A_{DCV}) of AAIW (A_{aaiw}) is seen
616 to form along the Moroccan coast, to drift southwestward and interact with meddies near
617 the Gulf of Cádiz. The A_{aaiw} is a tall lens of cold and fresh water. It has approximately
618 the same radius as the A_{meddy} and their interactions lead to substantial changes in their
619 respective trajectories.
620

621 Secondly, we observed the formation of cyclonic DCVs (C_{DCV_s}) near the African coast
622 ($C_{african}$) between 10°N and 25°N. Northward currents flow along the coast and cyclonic
623 vorticity is formed by friction. The $C_{african}$ detach from capes and promontories along
624 the coast (D'Asaro, 1988a). Afterwards, these $C_{african}$ drift northwestward, encounter the
625 $A_{meddies}$ with which they form dipoles. These dipoles accelerate the motion of the $A_{meddies}$
626 often in a chaotic manner with abrupt changes in the orientation of the trajectories. The
627 internal structures of the A_{meddy} and of the $C_{african}$ do not substantially change during
628 these interactions. It must be noted that, in the long run, the internal structures (radius,
629 thickness, temperature and salinity anomalies) of the A_{meddy} and the $C_{african}$ weaken due
630 to their interaction with heterogeneous background waters and due to their slow diffusion.
631 Furthermore, multiple interactions between such deep vortices have been found to tear fila-
632 ments away from them and thus to weaken them.
633

634 Thirdly, we have found that the A_{meddy} we studied can form a doublet with an A_{DCV}
635 generated near the Canary islands (A_{canary}). The A_{meddy} and the A_{canary} co-exist twice in
636 their lifetime. The interactions take place after the A_{meddy} has formed a dipole with the first
637 $C_{african}$ and after the last interaction of A_{meddy} with $C_{african}$. The doublet contributes
638 to a change in their orientation, and temporarily the A_{canary} forms an asymmetric tripole
639 with the A_{meddy} and a $C_{african}$. The vertical extent of the A_{canary} and the $C_{african}$ is 2000
640 m and their cores lie at 1500 m depth, they have radii of 40 km and 20 km, respectively,
641 and the A_{canary} has a salinity of 35.4 g/kg and a temperature of 8°C inside its core.
642

643 Finally, the A_{meddy} moves southwards, loses its salt and heat content as it undergoes
644 lateral intrusions (Armi et al., 1989) and it leaves a train of salty and warm water in its
645 wake. The shear flow created in between the A_{canary} creates disruption in the core of the
646 A_{meddy} finally leading to its destruction.

647 As a final conclusion, we indicate that the $A_{meddies}$ advect salt and heat over large
648 distances; they slowly mix these tracers with the surrounding water masses during the
649 meddy life cycle. This is a typical behaviour of the $A_{meddies}$ and their influence on the
650 $C_{meddies}$ often leads to the latter's destruction or splitting. Further, the $A_{meddies}$ interact
651 with other C_{DCV_s} or A_{DCV_s} throughout their journey. A more detailed analysis of these
652 eddy generation mechanisms, and of their nonlinear interactions during their life cycle, is
653 the subject of ongoing studies.

654 Open Research

655 The CROCO ocean model is available at `https://www.croco-ocean.org`. The CROCO
656 source code and configuration files used for the GIGATL simulations are available at `https://`
657 `github.com/Mesharou/GIGATL`. The *py-eddy-tracker* code used in this study is available at
658 `https://github.com/Mesharou/py-eddy-tracker`.

Acknowledgments

This work is funded by a Ph.D grant of the French CNRS (Centre National de la Recherche Scientifique). We would like to acknowledge support from the French National Agency for Research (ANR) through the project DEEPER (ANR-19-CE01-0002-01), from PRACE and GENCI for awarding access to HPC resources Joliot-Curie Rome and SKL from GENCI-TGCC (Grants 2022-A0090112051, 2021-A0090112051, 2020-A0090112051, 2019gch0401 and PRACE project 2018194735), and from HPC facilities DATARMOR of "Pôle de Calcul Intensif pour la Mer" at Ifremer Brest France. We thank Antoine Delepoulle , Clément Vic, Dante C. Napolitano, Josué Martinez Moreno, Manita Chouksey, and Sally Close for their valuable comments and feedback.

Appendix A

Distribution of detections in Rossby number and radius space

The distribution of detections with Rossby number (Ro) and radius (r) is shown in Figure 18 for vortices with a minimum lifetime of 21 days along isopycnal 27.60 kg/m^3. The black lines indicate the criteria $r = 15$ km and $Ro = 0.1$, which are used to define the large and energetic DCVs.

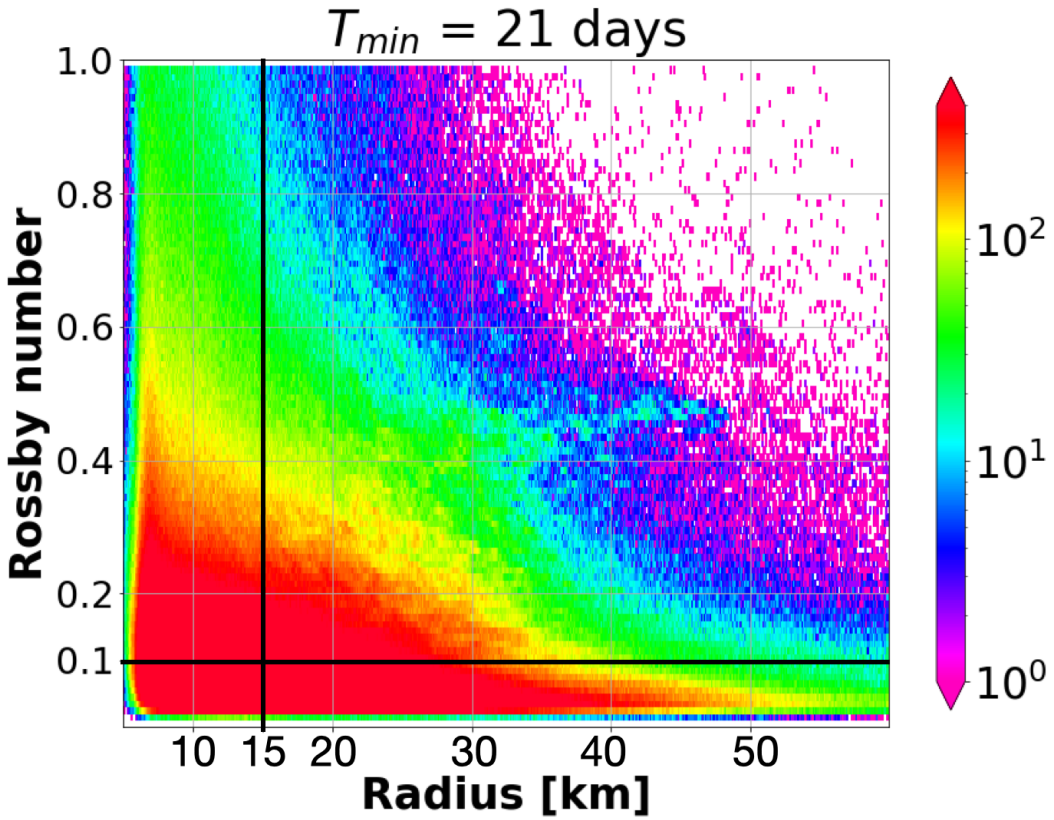

Figure 18. Number of detections as a function of Rossby number (Ro) and radius (r, in km).

Probability of sampling an anticyclone

The probability of finding anticyclonic DCVs (A_{DCV_s}) in the Northeast Atlantic is shown in Figure 19. It corresponds to the fraction of the area covered by A_{DCV_s} on average

within each bin.

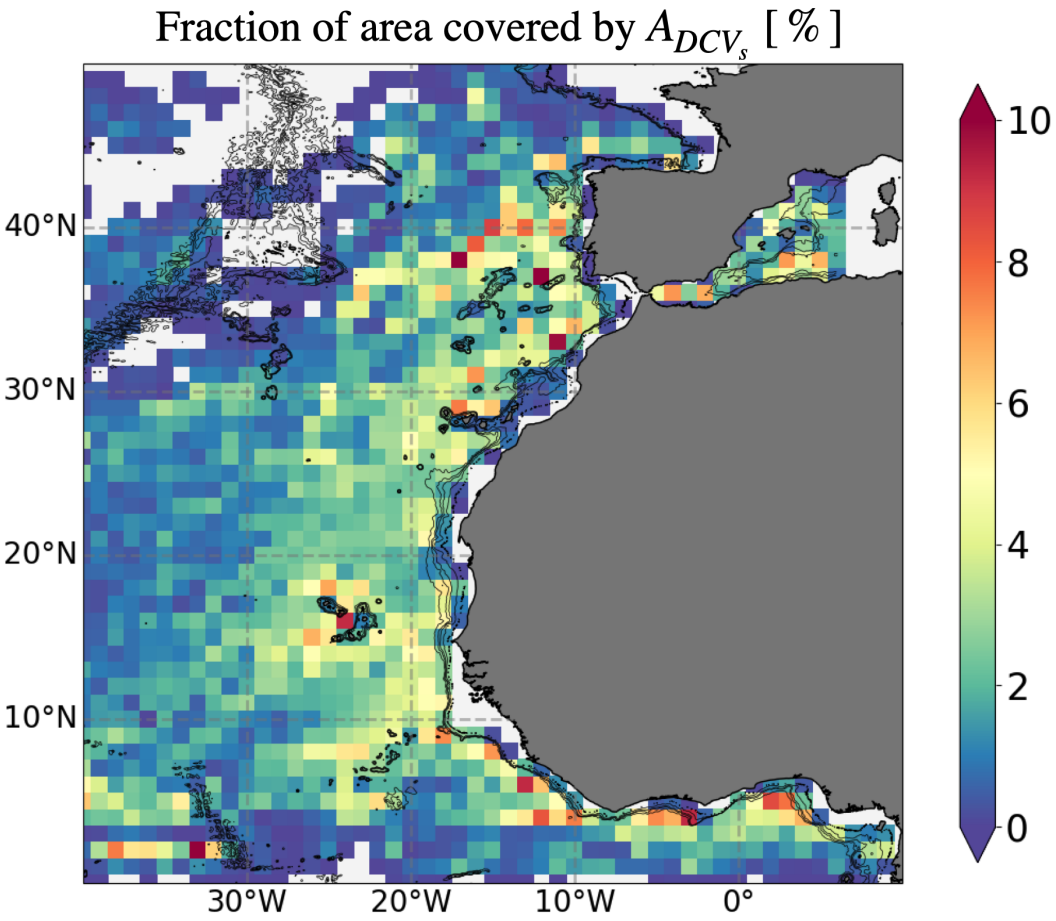

Figure 19. Fraction of the area covered by anticyclonic DCVs (A_{DCV_s}) living > 21 days and having Rossby number > 0.1 and radius > 15 km for at least half of their lifetime. The superimposed black contours with gray scale are the regions where the isopycnal exists $< 10\%$ in the simulation. The superimposed black contours are isobaths at 2000 m, 2500 m, 2700, and 3000 m.

Evolution of salinity in the Meddy core

The A_{meddy} shown in Figure 11a undergoes a slow increase in core salinity after crossing 20°N to the south. The structure and evolution of the A_{meddy} south of 20°N are illustrated here with horizontal maps and vertical sections of normalized relative vorticity and of salinity (Figure 20).

Note that t here, is the time in days after this A_{meddy} has reached 20°N and has already lived for 1292.5 days. The core of the meddy is concentrated between $1000 - 1500$ m depth, but its dynamic signal extends much further down. The vertical sections and profiles shown in Figure 20 cross the vorticity maximum. The vertical profiles of salinity along the vorticity maximum or the averaged value within the vorticity core are similar. While the volume-integrated salinity steadily decreases by slowing mixing with the fresher surrounding waters, changes in the vertical structure of the A_{meddy} induce an extension of the saline core

692 towards the isopycnal 27.60 kg/m^3.
693

694 **Generation of an African cyclone**

695 Successive snapshots of ζ/f and potential vorticity (PV) are shown in Figure 21 for the
696 $C_{african}$③. The plots from (a) to (l) are separated by five day intervals. The first snapshot
697 (a-c) corresponds to the moment when the $C_{african}$③ is born; it is followed by snapshots
698 after five days (d-f), 10 days (g-i), 15 days (j-l), 20 days (m-o), and after 55 days (p-r), when
699 the $C_{african}$③ is fully grown ($r > 15$ km).

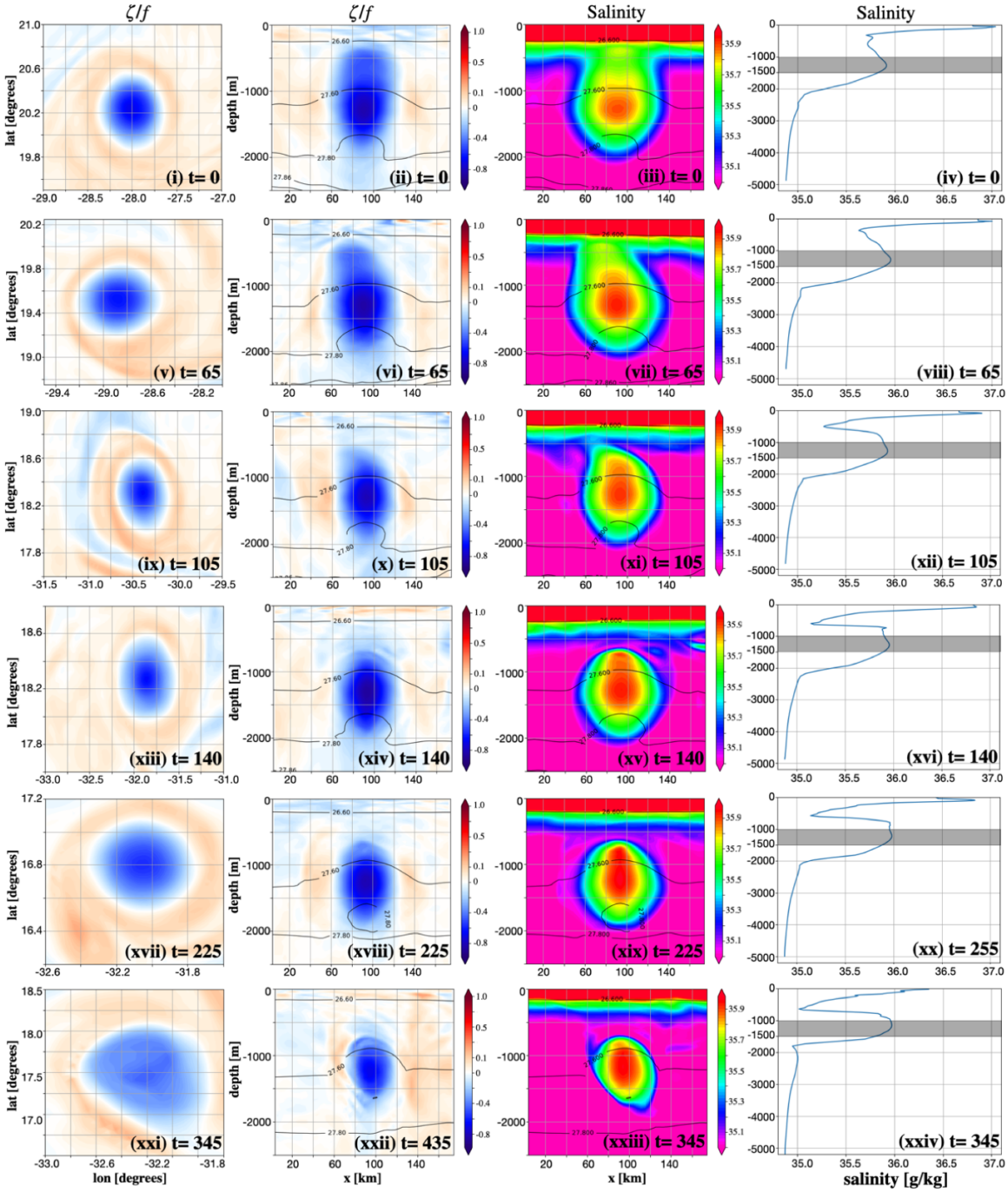

Figure 20. Horizontal maps of ζ/f (1st column) along the isopycnal 27.60 kg/m^3, vertical sections of ζ/f (2nd column), salinity (in g/kg) (3rd column), and vertical profile of salinity (in g/kg) (4th column). t denotes time in days. $t = 0$ refers to day 1292.5 of the anticyclonic meddy life. The superimposed black contours in the 2nd and 3rd columns refer to the isopycnal surfaces in kg/m^3. The grey strip in the 4th column refers to the depth of the 27.60 kg/m^3 isopycnal.

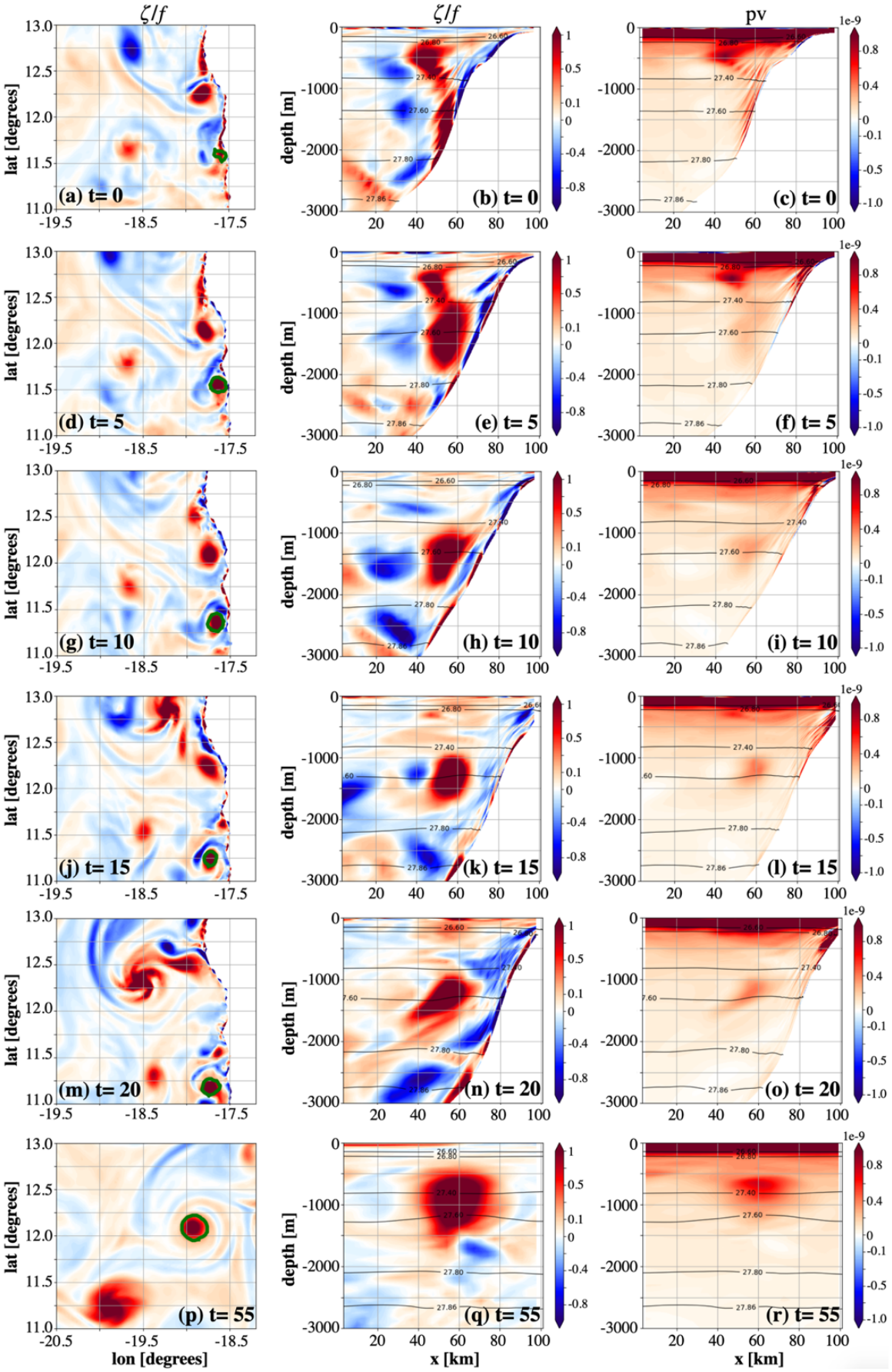

Figure 21. Generation of $C_{african}$ ③ in six steps shown by horizontal maps of ζ/f along the isopycnal 27.60 kg/m^3 (1st column), and by vertical sections of normalized relative vorticity (2nd column), and potential vorticity (PV) (3rd column). The snapshots refer to the model outputs; the overlaid contour in green denotes the eddy detection by the *py-eddy-tracker*; and the black contours in the 2nd and 3rd columns refer to the isopycnal surfaces in kg/m^3.

References

Aguiar, A., Peliz, Á., & Carton, X. (2013). A census of Meddies in a long-term high-resolution simulation. *Progress in Oceanography*, *116*, 80–94.

Ambar, I., Serra, N., Brogueira, M., Cabeçadas, G., Abrantes, F., Freitas, P., ... Gonzalez, N. (2002). Physical, chemical and sedimentological aspects of the Mediterranean outflow off Iberia. *Deep Sea Research Part II: Topical Studies in Oceanography*, *49*(19), 4163–4177.

Ambar, I., Serra, N., Neves, F., & Ferreira, T. (2008). Observations of the Mediterranean Undercurrent and eddies in the Gulf of Cadiz during 2001. *Journal of Marine Systems*, *71*(1-2), 195–220.

Arai, M., & Yamagata, T. (1994). Asymmetric evolution of eddies in rotating shallow water. *Chaos: An Interdisciplinary Journal of Nonlinear Science*, *4*(2), 163–175.

Arhan, M., Colin De Verdiére, A., & Mémery, L. (1994). The eastern boundary of the subtropical North Atlantic. *Journal of Physical Oceanography*, *24*(6), 1295–1316.

Armi, L., Hebert, D., Oakey, N., Price, J. F., Richardson, P. L., Rossby, H. T., & Ruddick, B. (1989). Two years in the life of a Mediterranean salt lens. *Journal of Physical Oceanography*, *19*(3), 354–370.

Bashmachnikov, I., & Carton, X. (2012). Surface signature of Mediterranean water eddies in the Northeastern Atlantic: effect of the upper ocean stratification. *Ocean Science*, *8*(6), 931–943.

Becker, J. J., Sandwell, D. T., Smith, W. H. F., Braud, J., Binder, B., Depner, J., ... Weatherall, P. (2009, November). Global Bathymetry and Elevation Data at 30 Arc Seconds Resolution: SRTM30_PLUS. *Mar. Geod.*, *32*(4), 355–371. doi: 10.1080/01490410903297766

Beckmann, A., & Käse, R. H. (1989). Numerical simulation of the movement of a Mediterranean water lens. *Geophysical research letters*, *16*(1), 65–68.

Canuto, V. M., Howard, A., Cheng, Y., & Dubovikov, M. (2001). Ocean turbulence. Part I: One-point closure model—Momentum and heat vertical diffusivities. *Journal of Physical Oceanography*, *31*(6), 1413–1426.

Carracedo, L., Gilcoto, M., Mercier, H., & Pérez, F. F. (2014). Seasonal dynamics in the Azores–Gibraltar Strait region: A climatologically-based study. *Progress in Oceanography*, *122*, 116–130.

Carracedo, L., Pardo, P. C., Flecha, S., & Pérez, F. F. (2016). On the Mediterranean water composition. *Journal of Physical Oceanography*, *46*(4), 1339–1358.

Carracedo, L., Pardo, P. C., Villacieros-Robineau, N., De la Granda, F., Gilcoto, M., & Pérez, F. F. (2012). Temporal changes in the water mass distribution and transports along the 20 W CAIBOX section (NE Atlantic). *Ciencias Marinas*, *38*(1b), 263–286.

Carton, J. A., & Giese, B. S. (2008). A reanalysis of ocean climate using simple ocean data assimilation (soda). *Monthly weather review*, *136*(8), 2999–3017.

Carton, X., Chérubin, L., Paillet, J., Morel, Y., Serpette, A., & Le Cann, B. (2002). Meddy coupling with a deep cyclone in the Gulf of Cadiz. *Journal of Marine Systems*, *32*(1-3), 13–42.

Carton, X., Le Cann, B., Serpette, A., & Dubert, J. (2013). Interactions of surface and deep anticyclonic eddies in the Bay of Biscay. *Journal of Marine Systems*, *109*, S45–S59.

Casanova-Masjoan, M., Pérez-Hernández, M. D., Vélez-Belchí, P., Cana, L., & Hernández-Guerra, A. (2020). Variability of the Canary Current Diagnosed by Inverse Box Models. *Journal of Geophysical Research: Oceans*, *125*(8), e2020JC016199.

Chelton, D. B., Schlax, M. G., & Samelson, R. M. (2011). Global observations of nonlinear mesoscale eddies. *Progress in oceanography*, *91*(2), 167–216.

Chelton, D. B., Schlax, M. G., Samelson, R. M., & de Szoeke, R. A. (2007). Global observations of large oceanic eddies. *Geophysical Research Letters*, *34*(15).

Chérubin, L., Carton, X., & Dritschel, D. (2007). Vortex dipole formation by baroclinic instability of boundary currents. *Journal of physical oceanography*, *37*(6), 1661–1677.

Chérubin, L., Carton, X., Paillet, J., Morel, Y., & Serpette, A. (2000). Instability of the mediterranean water undercurrents southwest of portugal: effects of baroclinicity and

of topography. *Oceanologica Acta*, *23*(5), 551–573.

D'Asaro, E. A. (1988a). Generation of submesoscale vortices: A new mechanism. *Journal of Geophysical Research: Oceans*, *93*(C6), 6685–6693.

D'Asaro, E. A. (1988b). Observations of small eddies in the Beaufort Sea. *Journal of Geophysical Research: Oceans*, *93*(C6), 6669–6684.

de Marez, C., Le Corre, M., & Gula, J. (2021). The influence of merger and convection on an anticyclonic eddy trapped in a bowl. *Ocean Modelling*, *167*, 101874.

Duarte, R., Carton, X., Capet, X., & Chérubin, L. (2011). Trapped instability and vortex formation by an unstable coastal current. *Regular and Chaotic Dynamics*, *16*(6), 577–601.

Ebbesmeyer, C. C., Taft, B. A., Mcwilliams, J. C., Shen, C. Y., Riser, S. C., Rossby, H. T., ... Östlund, H. G. (1986). Detection, structure, and origin of extreme anomalies in a Western Atlantic oceanographic section. *Journal of Physical Oceanography*, *16*(3), 591–612.

Gula, J., Theetten, S., Cambon, G., & Roullet, G. (2021, June). *Description of the GIGATL simulations.* Zenodo. Retrieved from `https://doi.org/10.5281/zenodo.4948523` doi: 10.5281/zenodo.4948523

Ingham, M. C. (1970). Coastal Upwelling in the Northwestern Gulf of Guinea. *Bulletin of Marine Science*, *20*(1), 1–34.

Johnson, J., & Stevens, I. (2000). A fine resolution model of the eastern North Atlantic between the Azores, the Canary Islands and the Gibraltar Strait. *Deep Sea Research Part I: Oceanographic Research Papers*, *47*(5), 875–899.

Käse, R. H., Beckmann, A., & Hinrichsen, H.-H. (1989). Observational evidence of salt lens formation in the Iberian Basin. *Journal of Geophysical Research: Oceans*, *94*(C4), 4905–4912.

Kostianoy, A., & Belkin, I. (1989). A survey of observations on intrathermocline eddies in the world ocean. In *Elsevier oceanography series* (Vol. 50, pp. 821–841). Elsevier.

Kurian, J., Colas, F., Capet, X., McWilliams, J. C., & Chelton, D. B. (2011). Eddy properties in the California Current System. *Journal of Geophysical Research: Oceans*, *116*(C8).

Louarn, E., & Morin, P. (2011). Antarctic Intermediate Water influence on Mediterranean Sea Water outflow. *Deep Sea Research Part I: Oceanographic Research Papers*, *58*(9), 932–942.

Machín, F., & Pelegrí, J. L. (2009). Northward penetration of antarctic intermediate water off northwest africa. *Journal of Physical Oceanography*, *39*(3), 512–535.

Mason, E., Colas, F., Molemaker, J., Shchepetkin, A. F., Troupin, C., McWilliams, J. C., & Sangrà, P. (2011). Seasonal variability of the Canary Current: A numerical study. *Journal of Geophysical Research: Oceans*, *116*(C6).

Mason, E., Pascual, A., & McWilliams, J. C. (2014). A New Sea Surface Height–Based Code for Oceanic Mesoscale Eddy Tracking. *Journal of Atmospheric and Oceanic Technology*, *31*(5), 1181–1188.

McCoy, D., Bianchi, D., & Stewart, A. L. (2020). Global observations of submesoscale coherent vortices in the ocean. *Progress in Oceanography*, *189*, 102452.

McDowell, S. E., & Rossby, H. T. (1978). Mediterranean Water: An Intense Mesoscale Eddy off the Bahamas. *Science*, *202*(4372), 1085–1087.

McWilliams, J. C. (1985). Submesoscale, coherent vortices in the ocean. *Reviews of Geophysics*, *23*(2), 165–182.

Okubo, A. (1970). Horizontal dispersion of floatable particles in the vicinity of velocity singularities such as convergences. In *Deep sea research and oceanographic abstracts* (Vol. 17, pp. 445–454).

Pegliasco, C., Delepoulle, A., Mason, E., Morrow, R., Faugère, Y., & Dibarboure, G. (2022). META3. 1exp: a new global mesoscale eddy trajectory atlas derived from altimetry. *Earth System Science Data*, *14*(3), 1087–1107.

Pelegrí, J., Arístegui, J., Cana, L., González-Dávila, M., Hernández-Guerra, A., Hernández-León, S., ... Santana-Casiano, M. (2005). Coupling between the open ocean and the

coastal upwelling region off northwest Africa: water recirculation and offshore pumping of organic matter. *Journal of Marine Systems*, *54*(1-4), 3–37.

Peña-Izquierdo, J., Pelegrí, J. L., Pastor, M. V., Castellanos, P., Emelianov, M., Gasser, M., ... Vázquez-Domínguez, E. (2012). The continental slope current system between Cape Verde and the Canary Islands. *Sci. Mar*, *76*, 65–78.

Perrot, X., & Carton, X. (2010). 2D vortex interaction in a non-uniform flow. *Theoretical and Computational Fluid Dynamics*, *24*(1), 95–100.

Pichevin, T., & Nof, D. (1996). The eddy cannon. *Deep Sea Research Part I: Oceanographic Research Papers*, *43*(9), 1475–1507.

Richardson, P., Bower, A., & Zenk, W. (2000). A census of Meddies tracked by floats. *Progress in Oceanography*, *45*(2), 209–250.

Saha, S., Moorthi, S., Pan, H.-L., Wu, X., Wang, J., Nadiga, S., ... others (2010). The NCEP Climate Forecast System Reanalysis. *Bulletin of the American Meteorological Society*, *91*(8), 1015–1058.

Sangrà, P., Pascual, A., Rodríguez-Santana, Á., Machín, F., Mason, E., McWilliams, J. C., ... Auladell, M. (2009). The Canary Eddy Corridor: A major pathway for long-lived eddies in the subtropical North Atlantic. *Deep Sea Research Part I: Oceanographic Research Papers*, *56*(12), 2100–2114.

Schütte, F., Brandt, P., & Karstensen, J. (2016). Occurrence and characteristics of mesoscale eddies in the tropical northeastern Atlantic Ocean. *Ocean Science*, *12*(3), 663–685.

Shchepetkin, A. F., & McWilliams, J. C. (2005). The regional oceanic modeling system (ROMS): a split-explicit, free-surface, topography-following-coordinate oceanic model. *Ocean modelling*, *9*(4), 347–404.

Solodoch, A., Stewart, A. L., & McWilliams, J. C. (2021). Formation of anticyclones above topographic depressions. *Journal of Physical Oceanography*, *51*(1), 207–228.

Srinivasan, K., McWilliams, J. C., Molemaker, M. J., & Barkan, R. (2019). Submesoscale vortical wakes in the lee of topography. *Journal of Physical Oceanography*, *49*(7), 1949–1971.

Umlauf, L., & Burchard, H. (2003). A generic length-scale equation for geophysical turbulence models. *Journal of Marine Research*, *61*(2), 235–265.

Weiss, J. (1991). The dynamics of enstrophy transfer in two-dimensional hydrodynamics. *Physica D: Nonlinear Phenomena*, *48*(2-3), 273–294.